DESIGN OF PATTERN RECONFIGURABLE ANTENNAS BY USING CHARACTERISTIC MODE THEORY

A THESIS SUBMITTED TO
THE GRADUATE SCHOOL OF NATURAL AND APPLIED SCIENCES
OF
MIDDLE EAST TECHNICAL UNIVERSITY

BY

TOLUNAY AYDIN

IN PARTIAL FULFILLMENT OF THE REQUIREMENTS
FOR
THE DEGREE OF MASTER OF SCIENCE
IN
ELECTRICAL AND ELECTRONICS ENGINEERING

SEPTEMBER 2020

Approval of the thesis:

DESIGN OF PATTERN RECONFIGURABLE ANTENNAS BY USING CHARACTERISTIC MODE THEORY

submitted by **TOLUNAY AYDIN** in partial fulfillment of the requirements for the degree of **Master of Science in Electrical and Electronics Engineering Department, Middle East Technical University** by,

Prof. Dr. Halil Kalıpçılar
Dean, Graduate School of **Natural and Applied Sciences** _____

Prof. Dr. İlkay Ulusoy
Head of Department, **Electrical and Electronics Engineering** _____

Assoc. Prof. Dr. Lale Alatan
Supervisor, **Electrical and Electronics Engineering, METU** _____

Examining Committee Members:

Prof. Dr. Sencer Koç
Electrical and Electronics Engineering, METU _____

Assoc. Prof. Dr. Lale Alatan
Electrical and Electronics Engineering, METU _____

Prof. Dr. Gülbin Dural
Electrical and Electronics Engineering, METU _____

Prof. Dr. Hatice Özlem Aydın Çivi
Electrical and Electronics Engineering, METU _____

Prof. Dr. Vakur Behçet Ertürk
Electrical and Electronics Engineering, Bilkent University _____

Date: 23.09.2020

I hereby declare that all information in this document has been obtained and presented in accordance with academic rules and ethical conduct. I also declare that, as required by these rules and conduct, I have fully cited and referenced all material and results that are not original to this work.

Name, Surname: Tolunay Aydın

Signature :

ABSTRACT

DESIGN OF PATTERN RECONFIGURABLE ANTENNAS BY USING CHARACTERISTIC MODE THEORY

Aydın, Tolunay
M.Sc, Electrical and Electronics Engineering
Supervisor: Assoc. Prof. Dr. Lale Alatan

September 2020, 71 pages

Pattern reconfigurable antennas improve the performance of the system in applications which have dynamic radiation pattern requirements like multi-input multi-output arrays, phased arrays and body area networks. Characteristic mode theory was shown to be useful when investigating the possible orthogonal radiation patterns on an antenna element. Due to improvements in computation capacity of the modern computers, characteristic mode analysis can be used efficiently during the design of pattern reconfigurable antennas. Several types of methods are proposed to excite distinct orthogonal modes on an antenna element in the literature. However, the fundamental idea behind all of these methods can be classified as either excitation by capacitive couplers or excitation by inductive couplers. The main drawback of these methods is their complexity in terms of fabrication. This work proposes a novel method for the excitation of different characteristic modes using only the microstrip feed lines so that the fabrication process can be simplified substantially. The proposed method is optimized for the chosen frequency range and simulated. The radiation patterns of realized configurations are measured and compared with the simulation results. Similarities and discrepancies are discussed. Finally, alternative excitation topologies are illustrated as the possible future work.

Keywords: Characteristic Modes, Square Patch Antenna, MIMO Antenna Element Design, Pattern Reconfiguration, Beam Steering

ÖZ

KARAKTERİSTİK MOD TEORİSİNİ KULLANARAK ÖRÜNTÜSÜ DEĞİŞTİRİLEBİLİR ANTEN TASARIMI

Aydın, Tolunay
Yüksek Lisans, Elektrik Elektronik Mühendisliği Bölümü
Tez Danışmanı: Doç. Dr. Lale Alatan

Eylül 2020, 71 sayfa

Işınım örüntüsü yeniden ayarlanabilen antenler MIMO diziler, faz dizili antenler, ve vücut tarama ağları gibi dinamik ışınım deseni gerektiren uygulamalarda sistemin performansını iyileştirmektedir. Karakteristik mod teorisinin bir anten elemanının olası ışınım desenlerine incelemede kullanışlı olduğu görülmüştür. Modern bilgisayarların işlem gücünün iyileşmesi sayesinde ışınım örüntüsü yeniden ayarlanabilen antenlerin karakteristik modların daha etkin kullanılarak tasarımı mümkün olmuştur. Literatürde ayrı karakteristik modları uyarmak için çeşitli farklı yöntemler önerilmiştir. Fakat temelde bu yöntemler kapasitif ekileşimle uyartı ve indüktif etkileşimle uyartı olmak üzere iki şekilde sınıflandırılabilir. Bu yöntemlerin ana dezavantajı üretim yönünden karmaşıklığıdır. Bu tezde yalnızca mikroşerit hatlar kullanılarak farklı karakteristik modların uyarımı için yeni bir yöntem önerilmiştir ve bu sayede üretim işlemi ciddi şekilde kolaylaştırılmıştır. Önerilen yöntem seçilen frekans aralığı için optimize edildikten sonra simüle edilmiştir. Gerçeklenen konfigürasyonların ışınım örüntüleri ölçülmüş ve simülasyon sonuçlarıyla karşılaştırılmıştır. Sonuçlardaki benzerlikler ve aykırılıklar tartışılmıştır ve en sonunda gelecekte çalışılmak üzere alternatif uyarım yapıları sunulmuştur.

Anahtar Kelimeler: Karakteristik Modlar, Kare Yama Anten, MIMO Anten Eleman Tasarımı, Örüntü Değiştirme, Hüzme Döndürme

ACKNOWLEDGMENTS

I would like to express my very gratitude and appreciation to my supervisor Assoc. Prof. Dr. Lale Alatan for her guidance, support and patience since the beginning of this study.

I would like to offer my special thanks to Aselsan Inc. for allowing me to use necessary tools in the manufacturing and measurement stages.

I also would like to thank to staff of Professional Communication Design Division in Aselsan Inc. for their utmost support as well.

I am grateful to Metehan Çetin for his suggestions on using the simulation software more efficiently.

I would like to thank Feza Turgay Çelik for his help during the pattern measurements in anechoic chamber.

I am particularly grateful to Berkan Önal for his help throughout manufacturing stage.

I would like to express my deep gratitude to my dear friend Mert Kayış for his encouragement, friendship and support.

Finally, my special thanks go to my family for their support, motivation and love.

TABLE OF CONTENTS

LIST OF TABLES

TABLES

LIST OF FIGURES

FIGURES

LIST OF ABBREVIATIONS

BAN: Body Area Network

LOS: Line of Sight

MEC: Modal Excitation Coefficient

MIMO: Multi Input Multi Output

MoM: Method of Moments

MS: Modal Significance

TCM: Theory of Characteristic Modes

CHAPTER 1

INTRODUCTION

Communication systems developed tremendously in the past twenty years. The increasing popularity of the communication devices brought the demand for higher data transmission rates, reliable, fading immune and low latency communication. Moreover providing service for large number of users has become an important problem. Throughout these years different techniques have been studied to satisfy these demands such as adapting higher clock rates and multiple access methods. Although multiple access methods like Time Division Multiple Access (TDMA) and Frequency Division Multiple Access (FDMA) techniques brought some degree of diversity to the service providers, diversity in spatial domain is also required to further increase the channel capacities. To achieve this diversity goal Multiple Input Multiple Output (MIMO) systems are used.

As the demand for use of mobile communication networks in different environments crowded with various scattering objects such as urban areas, dense forests, rugged terrains, etc. increased, the multipath fading phenomenon have been observed to cause problems in single input single output systems. This phenomenon occurs when line of sight (LOS) path is not the only path between receiver and transmitter antennas. Scattered waves from objects and surrounding also impinge on the receiver antenna and incoming waves don't have to be necessarily in phase with LOS waves. So depending on the relative position of antennas received field might get stronger when the multipath waves are in phase with LOS waves or they might add destructively for out of phase case and completely nullified. This multipath fading can be minimized by making use of spatial diversity offered by MIMO systems.

Obviously, multipath fading prevention is not the only advantage of MIMO systems but also the increase in the channel capacity is made possible by making use of multiple antennas. As suggested in the famous formula proposed by Shannon [1], the channel capacity can be either linearly increased by increasing the bandwidth or it can

be increased logarithmically by increasing the SNR (signal to noise ratio). By making use of the multiple transmitter and receiver antennas, the collected data can be combined which results in a higher SNR thus increasing channel capacity. To be able to realize these abovementioned advantages in the most efficient manner, far field patterns of antennas should be "uncorrelated".

The correlation coefficient between two antenna elements is proportional to inner product of the individual far field patterns. Correlation coefficient is a measure of orthogonality of individual far field patterns as the inner product of fields implicate. In an ideal MIMO configuration, antenna elements are expected to have orthogonal radiation patterns to satisfy the low correlation criterion. Moreover, for mobile communication systems, the pattern requirements of MIMO array elements change with varying channel characteristics. In order to meet these dynamic requirements, pattern reconfigurable antennas are used.

There are also different types of applications where the element pattern reconfiguration can be useful such as in the case of phased arrays or massive MIMO arrays, where the direction of the main beam is steered. As it is well known, in an array the overall radiation pattern is the product of the array factor and the element pattern. Therefore even if the array factor is maximized at any direction desired, the overall pattern will still depend on the element's pattern. Furthermore, no matter what the array factor is, the overall pattern will have nulls at the nulls of the element pattern. Hence a pattern reconfigurable element would improve the performance of the array for different scan angles. For example, the antenna could have a broadside directed pattern when it is scanned to low angles from bore sight, whereas it could switch to a dipole like pattern when the beam is scanned to 70^0-90^0 from broadside.

Pattern reconfigurable antennas are also widely used in body are networks (BAN). In BAN, an on-body link collects data from sensors on the body and these data are sent to an external unit through an off-body link for monitoring. If same antenna is used for on-body and off-body links, an omni-directional pattern is required for whole coverage of the body during on-body communication and a directional pattern for off-body mode is preferred for higher gain. Therefore, pattern reconfigurable antennas are generally utilized in BAN.

Different approaches are employed to achieve pattern reconfiguration. Most widely utilized approach is to use parasitic elements in order to tilt the beam away from the broadside direction [2][3][4]. The second widely used approach is to combine different resonators in a single aperture so that different patterns could be achieved by exciting the corresponding resonator [5][6][7]. Both of these two approaches result in antennas with sizes larger than half wavelength due to the introduction of parasitic elements or extra resonators. However, in this thesis design of a pattern reconfigurable antenna to be used in phased array applications is considered. Therefore these two design approaches are not suitable for this thesis work due to the constraint on the size of the antenna. Recently the utilization of theory of characteristic modes (TCM) is proposed to design reconfigurable antennas. In this approach a single radiating structure is used but different modes are excited by using different excitation configurations. Since small size requirement could be satisfied with a single radiator, TCM is chosen to guide the design process in this thesis.

TCM is first proposed by Garbacz in 1968 [8], then it is further discussed by Harrington and Mautz in 1970 [9]. Harrington and Mautz derived an eigenvalue problem for a conducting object by transforming the corresponding E-field integral equation into a matrix equation through the use of Method of Moments (MoM). This eigenvalue problem is only a function of the conductor geometry and it does not involve any information about the excitation. The eigenvectors or namely eigencurrents are orthogonal to each other and consequently they form a complete basis that could represent any current distribution that could be excited on the conductor. As it will be defined later in this thesis, parameters like modal significance and characteristic angle which are derived from eigenvalues, provide information about how effectively a specific eigenmode could be excited. The set of radiation patterns corresponding to eigencurrents also form an orthogonal set. Therefore TCM is a very efficient tool that can be utilized in the design of pattern reconfigurable antennas. However due to the high computational cost of evaluating the eigenvalues and eigencurrents, TCM has not been widely used in antenna design until computers with high process speed and memory capacity became available.

In 2007 Cabedo M. had shown examples of the systematic design of the antennas using characteristic mode theory [10]. In her work she analyzed the characteristic mode currents for different type of antennas such as wire type, rectangular, triangular and circular patches and ground planes. Unlike Garbacz, Harrington and Mautz her work leans more on the physical interpretation of characteristic modes and gives methods to excite different modes on different type of antennas. She models each mode as a different resonator circuit and explains the concept of capacitive and inductive modes by using modal significance and characteristic angle values. Her work also contains matching structures with inductive and capacitive loading for each mode in detail.

In 2016 Manteuffel D. and Martens R. utilized TCM not to design a pattern reconfigurable antenna but to design a multi-mode antenna that will be used as an element in an indoor ultra-wideband massive MIMO array with 484 elements [11]. They fed the antennas using gap sources and to do so they needed to add rectangular slots to edges of each patch. In their work it is also shown that adding slots to edges or corners does not significantly disturb the original characteristic mode patterns of the square patch. Their work shows this by computing the envelope correlation coefficient between the characteristic mode patterns of square patches with and without slots and it turns out that minimum correlation is 0,7 out of 5 different characteristic modes of interest. Excitation configurations for each mode and matching techniques are explained in detail and they achieved to design a multi-mode antenna with high inter-port isolation and low return loss. The element sizes used in their design is a little bit less than ¾ wavelength and at the end of their work, possibility of further reduction of element's electrical size is discussed and conclusion turns out that it can be done only by sacrificing from inter-port isolation.

Use of capacitive parasitic plates in addition to the main radiating plate is proposed in [12]. First eigenvalues and eigenpatterns of first eight modes for a 120 mm x 60 mm rectangular plate at 2.45 GHz (corresponding almost λ x $\lambda/2$ in terms of electrical length) are investigated. Then, it is shown that additional parasitic elements can be placed in such a way that eigenvalues for each mode can be manipulated and the most significant mode at 2.45 GHz can be changed to another one with its main beam

rotated. Hence, it is shown that it is possible to rotate the main beam of the antenna at the same frequency by the help of additional parasitic plates. Exciting different sets of parasitic elements is made possible by adapting to suitable feeding structures where the feeding structures are switched by using pin diodes and each structure is used for exciting a different characteristic mode at the same frequency. Note that, although the most significant mode changes as parasitic plates are placed, the modal significance still can't get as high as the original fundamental mode. As their results suggest the second mode can only get a modal significance between 0.6-0.8 which directly diminishes the radiation efficiency. This reduction in the radiation efficiency will be also discussed further in this thesis, since the same problem occurs with single piece radiator type structures.

Using capacitive coupling elements is one way to achieve the excitation of different modes. Another method is using inductive coupling elements as shown by Dicandia and Genovesi in 2018 [13]. In the case of inductive coupled feeding, the well known method is forming one feeding loop on the main radiator. One end of the loop is connected to the radiator and the other end is connected to the source. However, this kind of coupling is called as unbalanced inductive coupling and it does not allow the excitation of different modes separately but rather it excites different modes simultaneously. To solve this problem they proposed a novel method called "balanced inductive elements" where the excitation elements consist of two loops instead of a single loop and these two loops are fed with an adjustable phase difference. By doing so they increased the modal purity of their topology meaning that they became able to excite the particular mode of interest. They also compare the radiated and reactive powers for two topologies and show a significant improvement for radiation efficiency of all modes when balanced inductive elements are used as exciters. One may wonder the possibility of radiation of inductive these loops, however they express the electrical sizes of loops are so small that they won't disturb the far field pattern of the main radiator and final radiation pattern results support their claim.

Martens and Safin [14] simulated the excitation cases for both the capacitive and inductive coupler exciters in 2011. A rectangular PCB is considered as a main radiator and the PCB is fed from its corners and by capacitive coupling elements to excite three

different characteristic modes separately. Then PCB is fed by inductive coupling elements placed at the middle of edges to excite the same modes. The results turned out to be both options are viable. However, the modal purity of the capacitive coupled excitation case turned out to be a little lower than inductive coupled excitation case. They explain this situation due to the fact that all three modes possess maxima of the E-field. Capacitive or inductive coupling elements achieve the excitation of different characteristic modes, but their implementation becomes more difficult as the frequency of operation gets higher. Furthermore if the switches used for reconfiguration will be microelectromechanical systems (MEMS), and if same process will be used to manufacture the antenna and the switches, implementation of capacitive or inductive coupling elements would be much harder. Therefore in this thesis, the possibility and feasibility of exciting different characteristic modes by using simple proximity coupled microstrip feed lines will be investigated to ease the manufacturing process for higher frequency bands and different manufacturing processes.

A pattern reconfiguration approach similar to the one proposed in [12] is used by Kishor and Hum in 2013 [15]. Unlike [12], they did not only connect the parasitic elements to the main patch directly, but they also loaded these parasitic elements with lumped inductors in order to ensure minimum cross-correlation between the ports. In this case, main radiator is physically connected to inductive loads via pin diodes. In the off state of diodes the main radiator exhibits the pattern of one mode. Whenever the pin diodes are switched on, main antenna element practically changes its shape and exciting another orthogonal mode on the same rectangular patch becomes possible along with the lowest possible cross-correlation. Their work also demonstrates the behavior of eigenvalues in the presence of inductive/capacitive loading that shows which modes are more likely to be excited under the loading and which are not. It turns out that modes with the circular loop current distribution are more difficult to excite regardless of the parasitic plate configuration.

Another method is illustrated in 2014 by Miers Z. and Lau B.K [16]. They designed two different chassis configurations to adapt multimode in MIMO applications for handheld devices. Their work starts with demonstrating a regular flat rectangular

chassis which only supports a single mode. Then, instead of using separate parasitic plates, they cover the whole chassis with a metallic framework structure called "bezel" (side wall). Li and Shi used 4 different metallic plates to excite 4 different modes whereas adding a single bezel frame at the four sides of the rectangular chassis enables to excite only a different second mode at the same frequency. Another difference of this method is the lack of physical contact when compared to others. Bezel does not touch the chassis but there is some air gap between them. By doing so they provided a uniform shift with frequency for 2 alternative modes. Eventually, they optimized the feed point locations to obtain the best matching and the lowest coupling between the ports. Although, later they show it is possible to excite more than 2 modes simultaneously at the same frequency, it can be seen that they manipulated the original structure even more by adding extra resonating elements.

In [17] both a bi-directional and a directional pattern are obtained by placing two rectangular plates in parallel. When neither of the plates are excited the pattern exhibits a bi-directional behavior since the currents on two plates have the opposite direction like in the case of a transmission line, whereas when one of the plates are excited with an optimized probe feed, the currents flowing on the plate are aligned and this shifts the pattern to a directional one.

In 2014, S. Dumanlı proposed a method to excite two different cavity modes on a patch antenna to have both an omni-directional pattern for on-body link and a broadside directed pattern for off-body link at 2.4 GHz [18]. In this work, pattern reconfiguration is achieved by shorting a square patch on a ground plane from three different points by conducting vias. Two of these points are also used as the feeding points for the patch. It is shown that feeding these two points with equal phase yields an E-field distribution of TM_{00} mode and feeding them out of phase yields an E-field distribution of TM_{01} mode, hence she obtained two orthogonal radiation patterns at the same frequency. The phase difference at the feeding points is adjusted with changing the length of one branch by a switch. However, the two main challenge for such a configuration is the complexity of the production. Using conductive vias to connect ground plane and the patch is not very preferable in terms of fabrication when compared with using proximity coupled feeding scheme.

The investigated works up to this point have adapted to change their feeding topology either using switches or pin diodes. A different useful method is proposed by Chaudhury and Schroeder in 2012. Their configuration also requires both the in phase and out of phase feedings. Rather than manipulating the feed line lengths they suggest using hybrid couplers to apply the necessary phase shifts between the ports. The simplicity in the implementation is not the only advantage but hybrid couplers also provide an increased isolation between their ports which will help to further reduce the cross-correlation [19].

Although all of the aforementioned methods allow the pattern reconfiguration, all have some drawbacks when it comes to using them in phased arrays and to manufacture them by using MEMS production processes. They have sizes larger than half wavelength and adding extra parasitic plates or shorting vias along with some lumped loads on a main radiator makes it impractical to fabricate them using MEMS technology. In this study, there are two main goals that distinguish design criteria from the aforementioned methods. First goal is to design the element with a size less than half wavelength, so that it could be used in phased arrays. And the second requirement is on the structure of the antenna, it should be suitable to be manufactured together with MEMS switches.

In the second chapter, the main theory of characteristic modes is given with fundamental definitions and derivations. As a starting point first most significant four modes on a square patch will be examined. A commercially available MoM based full-wave electromagnetic analysis software, called FEKO [20], is used for characteristic mode analysis. After detailed examination of the modes, the most suitable characteristic modes will be chosen for pattern reconfigurable applications by comparing the resulting far field patterns. Afterwards, regular square patch shape will be manipulated to have wider bandwidth and same resonance frequency for the desired modes. For different type of shape manipulations, modal significance responses are compared and the most suitable shape is chosen. After the ideal shape is found, different feeding schemes are studied to excite the mode of interest. Then, the impedance matchings at the resonance frequencies are optimized. Different type

of feeding scenarios are discussed their benefits and drawbacks are compared. The feeding scheme to be manufactured is decided at the end of this chapter.

In the third chapter, electrical specification measurements of the manufactured antenna will be given. S-parameter measurements and radiation pattern measurements will be shown and final results will be compared with the ones obtained during the simulations.

At the fourth chapter, as a possible future work, use of rat-race couplers in the feeding structure is investigated through simulation results and the thesis is concluded.

CHAPTER 2

CHARACTERISTIC MODE ANALYSIS OF THE PATCH ANTENNA

2.1 Theory of Characteristic Modes

First of all, a rigorous derivation of the characteristic modes, as in [2], will be presented in this chapter in order to build a fundamental basis for the interpretation of eigenvalues and eigencurrents during the antenna design phase.

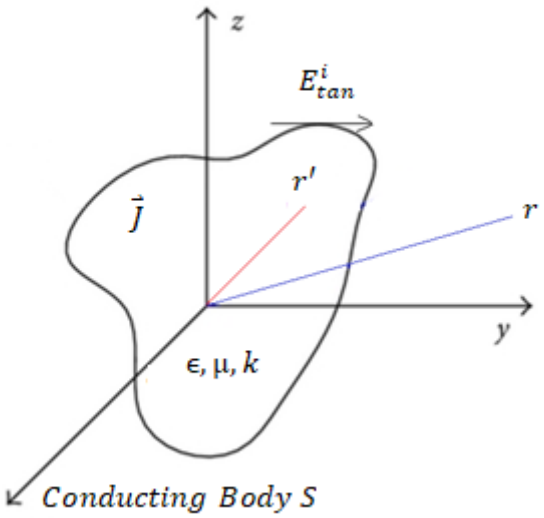

Figure 1. Arbitrary conducting body

When a conducting body like in Figure 1 is considered in an impressed electric field $\vec{E}^i$, and induced surface current density $\vec{J}$, according to the boundary conditions the following equation should be satisfied:

$$\left[L(\vec{J}) + \overrightarrow{E^i}\right]_{tan} = 0 \tag{1}$$

where L is an operator which represents the scattered electric field created by $\vec{J}$, and it can be written in terms of vector ($\vec{A}$) and scalar (V) potential functions as:

$$L(\vec{J}) = -j\omega\vec{A}(\vec{J}) - \vec{\nabla}\Phi(\vec{J}) \tag{2}$$

Potential functions are expressed in terms of current densities as:

$$A(\vec{J}) = \mu \oiint_S \vec{J}(\overrightarrow{r'})\psi(\vec{r},\overrightarrow{r'})ds' \tag{3}$$

$$\Phi(\vec{J}) = -\frac{1}{j\omega\epsilon} \oiint_S \nabla' . \vec{J}(\overrightarrow{r'})\, \psi(\vec{r},\overrightarrow{r'})ds' \tag{4}$$

where $\psi(\vec{r},\overrightarrow{r'})$ is the free space Green's function.

When the unit of L operator is examined it can be seen that it is Ω(V/cm/A/cm). So this operator is generally also denoted as $Z(\vec{J})$. Z is a symmetric operator and therefore its real and imaginary parts can be decomposed as in equations 5 and 6, respectively.

$$R = \frac{1}{2}(Z + Z^*) \tag{5}$$

$$X = \frac{1}{2j}(Z - Z^*) \tag{6}$$

R represents a measure of radiated power from the conducting body. X represents the stored energy and it can be positive, negative or zero depending on the capacitive or inductive behavior of the body.

A generalized eigenvalue problem can be defined by using the weighting operator, M:

$$Z(\vec{J}_n) = v_n M(\vec{J}_n) \tag{7}$$

where $\boldsymbol{v_n}$ is the nth eigenvalue and $\vec{J}_n$ is the corresponding eigenfunction (also called as eigencurrent or characteristic current). As shown in [9], the radiation patterns will be orthogonal if and only if $M = R$. So equation 7 is rewritten as:

$$(R + jX)(\vec{J}_n) = v_n R(\vec{J}_n) \tag{8}$$

Eigenvalues turn out to be:

$$v_n = 1 + j\lambda_n \tag{9}$$

Rearranging equation 8 yields:

$$X(\vec{J}_n) = \lambda_n R(\vec{J}_n) \tag{10}$$

Since X and R are real, all λ_n and $\vec{J}_n$ must be real as well. Moreover, $\vec{J}_n$ must also satisfy the following orthogonality relationships:

$$\left.\begin{aligned} <J_m, RJ_n> &= 0 \\ <J_m, XJ_n> &= 0 \\ <J_m, ZJ_n> &= 0 \end{aligned}\right\} \; m \neq n \tag{11}$$

Being a real function $\vec{J}_n^*$ satisfies the orthogonality conditions as well as shown in the following equation:

$$\left.\begin{aligned} <J_m^*, RJ_n> &= 0 \\ <J_m^*, XJ_n> &= 0 \\ <J_m^*, ZJ_n> &= 0 \end{aligned}\right\} \; m \neq n \tag{12}$$

In order to simplify the computations, all eigencurrents will be considered to be normalized as in equation 13 from this point on. Thus, the radiated power due to these eigencurrents will become unity.

$$<J_n^*, RJ_n> = 1 \tag{13}$$

The normalization relation can be combined with the orthogonality properties as in the equation set 14:

$$\left.\begin{aligned} <J_m, RJ_n> = <J_m^*, RJ_n> &= \delta_{mn} \\ <J_m, XJ_n> = <J_m^*, XJ_n> &= \lambda_n \delta_{mn} \\ <J_m, ZJ_n> = <J_m^*, ZJ_n> &= (1 + j\lambda_n)\delta_{mn} \end{aligned}\right\} \tag{14}$$

where δ_{mn} is the Kronecker-Delta function. It yields 0 as long as $m \neq n$, otherwise it is 1.

2.2 Numerical Computation of Eigenvalues and Eigencurrents with MoM

The Z operator acting on $\vec{J}$ can be converted to a matrix vector product by applying Method of Moments (MoM). First, $\vec{J}$ can be expressed in terms of basis functions w_j as:

$$\vec{J} = \sum_j I_j w_j \tag{15}$$

where I_j's are the constant coefficients of basis functions. Then the operator can be weighted by taking its inner product with testing functions. To obtain symmetric matrices, Galerkin's approach is used and the testing functions are chosen to be same as the basis functions. As a result $Z(\vec{J})$ operator is transformed to $[Z][I]$ where the entries of Z matrix are expressed as:

$$Z_{ij} = -\oiint_S ds' \oiint_S ds \left[j\omega\mu \overrightarrow{w_i}.\overrightarrow{w_j} + \frac{1}{j\omega\epsilon}\left(\vec{\nabla} \; .\overrightarrow{w_i}\right)\left(\vec{\nabla}'.\overrightarrow{w_j}'\right)\right]\psi \tag{16}$$

The free space Green's function can be decomposed into its real and imaginary parts to obtain R_{ij} and X_{ij}. Then the following eigenvalue problem can be obtained.

$$[X][I]_n = \lambda_n [R][I]_n \tag{17}$$

Note that $[Z]$ is the generalized impedance matrix of the conducting body and $[X]$ represents the reactive and $[R]$ represents the resistive parts of it. The orthogonality relation in operator form applies to the matrix form as well as it can be seen in the following equation.

$$< J_m \; , RJ_n > \; = [I]_m^T \, [R][I]_n = \delta_{mn} \tag{18}$$

2.3 Computation of Characteristic Fields and Patterns

The electric field $\vec{E}_n$ and magnetic field $\vec{H}_n$ created by the eigencurrents $\vec{J}_n$ on the conducting body S are called as characteristic fields or eigenfields. The orthogonality of $\vec{E}_n$ and $\vec{H}_n$ are derived from the complex power relations as in the following equations.

$$P = < J^*, ZJ > = < J^*, RJ > \ + j < J^*, XJ > \tag{19}$$

$$P = \oiint_{S'} \vec{E}\, x\, \vec{H}^* .\ d\vec{s} + j\omega \iiint_{\tau'} (\mu\vec{H} . \vec{H}^* - \epsilon\vec{E} . \vec{E}^*) d\tau \tag{20}$$

Where S' is any surface enclosing S and τ' is the region enclosed by S'.

When complex Poynting expression is written for a pair of eigencurrents, the expressions in the following equations are obtained.

$$P(\vec{J}_m, \vec{J}_n) = < J_m^*, ZJ_n > \tag{21}$$

$$\oiint_{S'} \vec{E}_m\, x\, \vec{H}_n^* .\ d\vec{s} + \ j\omega \iiint_{\tau'} (\mu\vec{H}_m . \vec{H}_n{}^* - \epsilon\vec{E}_m . \vec{E}_n{}^*) d\tau = (1 + j\lambda_n)\delta_{mn} \tag{22}$$

For a finite conducting body S, if the enclosing surface S' is chosen as a sphere with infinite radius, characteristic electric fields and magnetic fields will be in the form of outward travelling spherical waves as in the following equation:

$$\vec{E}_n = \eta\vec{H}_n\, x\, \vec{n} = \ -\frac{j\omega\mu}{4\pi r} e^{-jkr} \vec{F}_n(\theta, \phi) \tag{23}$$

where η represents the intrinsic impedance of the free space, $\vec{n}$ represents the radial unit vector on S' and (θ, ϕ) represent the elevation and azimuth angle respectively. $\vec{F}_n$ is called as the eigenpattern created by the eigencurrent $\vec{J}_n$. If complex conjugate of equation 22 is summed with itself, the following equations are obtained which provide the orthogonality relations between the characteristic electric fields and magnetic fields where S_∞ denotes the enclosing surface.

$$\frac{1}{\eta} \oiint_{S_\infty} \vec{E}_m . \vec{E}_n^* ds = \delta_{mn} \tag{24}$$

$$\eta \oiint_{S_\infty} \vec{H}_m . \vec{H}_n^* ds = \delta_{mn} \tag{25}$$

If complex conjugate of equation 22 is subtracted from itself, the eigenvalue relation between the characteristic fields is found as:

$$\omega \iiint \left(\mu \vec{H}_m \,.\, \vec{H}_n{}^* - \epsilon \vec{E}_m \,.\, \vec{E}_n{}^*\right) d\tau = \lambda_n \delta_{mn} \tag{26}$$

2.4 Modal Solutions

Modal solutions for the current density $\vec{J}$ on the conducting body S can be obtained by using the eigencurrents as both expansion and testing functions. So $\vec{J}$ will be a linear combination of eigencurrents as:

$$\vec{J} = \sum_n \alpha_n \vec{J}_n \tag{27}$$

When this expansion is substituted in equation 1, the following expression is obtained.

$$\left[\sum_n \alpha_n L\vec{J}_n + \vec{E}^i\right]_{tan} = 0 \tag{28}$$

By taking the inner product with $\vec{J}_m$ and using the Z matrix, the following equation is obtained.

$$\sum_n \alpha_n < J_m \,, ZJ_n > + < J_m \,, E^i > = 0 \tag{29}$$

When the orthogonality relations in equation 14 are used, modal excitation coefficients (V_n^i's), which are the inner product of the impressed electric field and the eigencurrent, are obtained as follows:

$$V_n^i = - < J_n \,, E^i > = \alpha_n (1 + j\lambda_n) \tag{30}$$

would be maximized.

When α_n values in equation 30 are substituted into equation 27, the mode expansion of surface currents density is obtained as:

$$\vec{J} = \sum_n \frac{V_n^i \vec{J}_n}{1 + j\lambda_n} \tag{31}$$

Note that, eigencurrents in equation 31 are considered to be normalized prior to the computation. It can be seen that, as an eigenvalues get larger in magnitude, the contribution of the corresponding characteristic mode gets smaller. Therefore a parameter is defined in terms of the eigenvalue to indicate how strong the corresponding mode can be excited. This parameter is called modal significance (MS) and it is defined as:

$$MS = \left| \frac{1}{1 + j\lambda_n} \right| \tag{32}$$

Note that MS is constrained in [0 1] interval and a mode with MS close to 1 (eigenvalue close to zero) will be excited more dominantly. A certain mode is considered to be radiating effectively as long as its MS is larger than 0.707 [10]. The mode of interest still radiates for smaller values of MS, but the radiated power diminishes substantially and the stored energy increases significantly which makes the body an inefficient radiator for that mode. Note that, MS is not the only parameter that determines the coefficient of a specific mode. From eqn. 31 it can be seen that modal excitation coefficient (MEC) also indicates how strong a mode is excited. The distinction between MS and MEC is that, MS depends only on the geometry and dimensions of the conducting body and frequency, whereas excitation mainly determines MEC. Hence to excite a mode with MS larger than 0.707 efficiently, excitation configuration should be designed carefully by inspecting the corresponding characteristic current distribution.

One can also investigate the eigenvalues to check the resonance situation of the corresponding mode. The sign of eigenvalues also indicate the type of the non-radiating modes. Positive eigenvalues correspond to inductive modes whereas negative eigenvalues correspond to capacitive modes. In order to decide whether the mode is inductive or capacitive, another parameter called characteristic angle (CA) is defined as:

$$CA = 180^0 - \tan^{-1}(\lambda_n), \qquad \tan^{-1}(\lambda_n) \ \epsilon \ [-90, 90] \tag{33}$$

If CA is greater than 180^0, the mode is called as a capacitive mode and if it is smaller than 180^0, it is called as an inductive mode. At exactly 180^0 mode is considered to be at resonance.

2.5 Investigation of the Characteristic Modes on a Square Patch Antenna

So far, all necessary definitions and derivations are given to design a pattern reconfigurable antenna element. The main goal is to be able to excite different eigenmodes with different patterns. Within the scope of this thesis two different radiation patterns are chosen. One of them is a uni-directional broadside pattern and the other one is a conical beam with a null at broadside. Since this element could be used in arrays with large number of elements, the elements should be small and inexpensive. The best candidate with such properties is the patch antenna. Considering planar array, a symmetric geometry with respect to x and y axis would be a logical choice. So, a square shaped patch antenna is considered to be the ideal one for such an application. The band of operation is chosen as sub-6 GHz. Since the aim of this thesis is to explore the possibility of using a simple feed network for the excitation of certain characteristic modes, a specific frequency is not chosen in order to avoid the extra effort to tune the antenna to the specified frequency. Once a design could be achieved through the methodology studied in this thesis, then the design can be tuned to desired frequency. The size of the patch is chosen as 32 mm x 32 mm on a RO4003C [21] substrate with the dielectric constant (ϵ_r) of 4.3 and thickness of 0.406 mm. Since operating frequencies are relatively low, RO4003C provides low enough loss tangent (around 0.0021).

The eigenvalues for the first four modes for this square patch on the grounded dielectric substrate are plotted in Figure 2. Note that due to the square shape, the curves for the first two modes overlap.

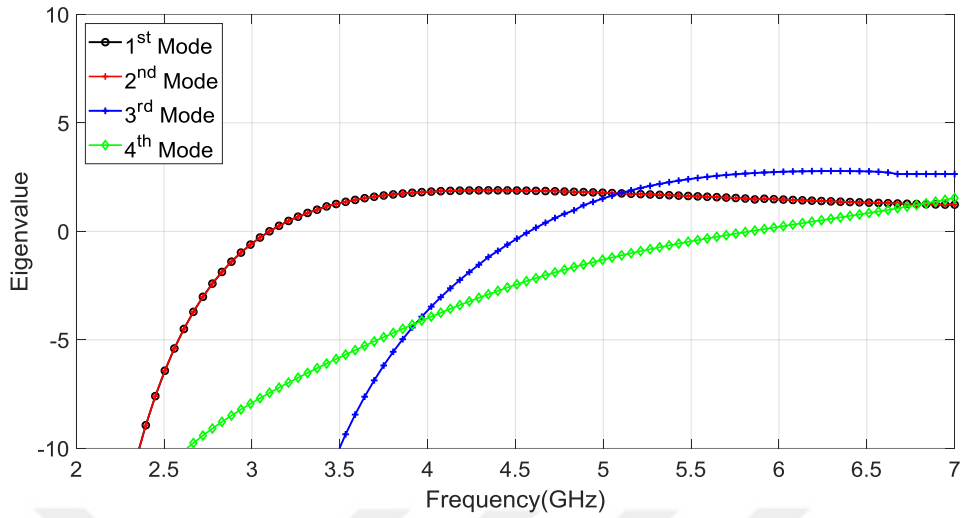

Figure 2. Eigenvalues of the first 4 modes vs. frequency for square patch

Figure 2 gives a general idea about how the related modes behave at frequencies up to 7 GHz. However, exact resonance frequencies can be seen more easily in Figure 3, which demonstrates MS values.

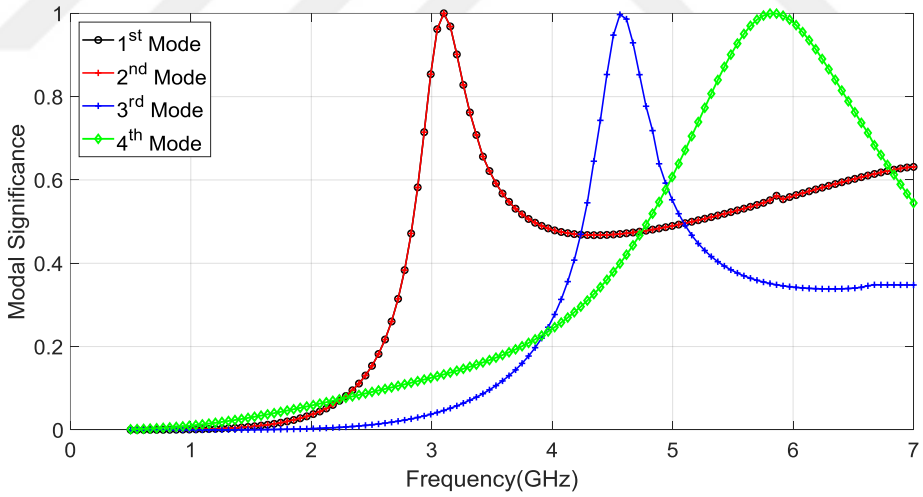

Figure 3. Modal significance of the first 4 modes vs. frequency for square patch

First two modes resonate at 3.12 GHz, the 3rd mode resonates at 4.60 GHz and the 4th mode resonates at 5.85 GHz. These four modes are not the only eigenmodes, infinitely many eigenmodes emerge as frequency gets higher. These four modes can be called as ‘’fundamental modes’’ [4]. Since higher order modes have resonance frequencies beyond the band we are interested in, they are not studied in detail.

Current distributions on the patch for the first four eigenmodes are given in Figure 4, Figure 5, Figure 6 and Figure 7, respectively.

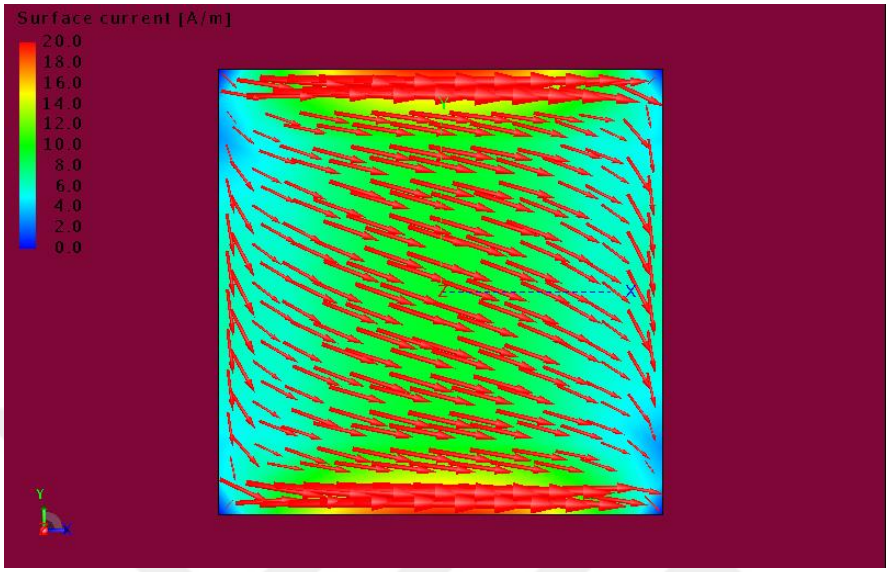

Figure 4. Current distribution of the 1st eigenmode on square patch at 3.12 GHz

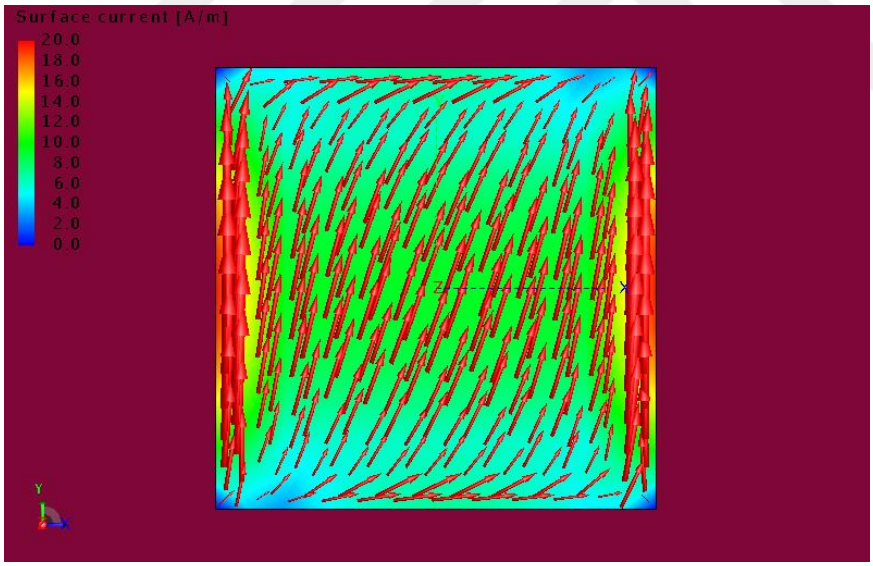

Figure 5. Current distribution of the 2nd eigenmode on square patch at 3.12 GHz

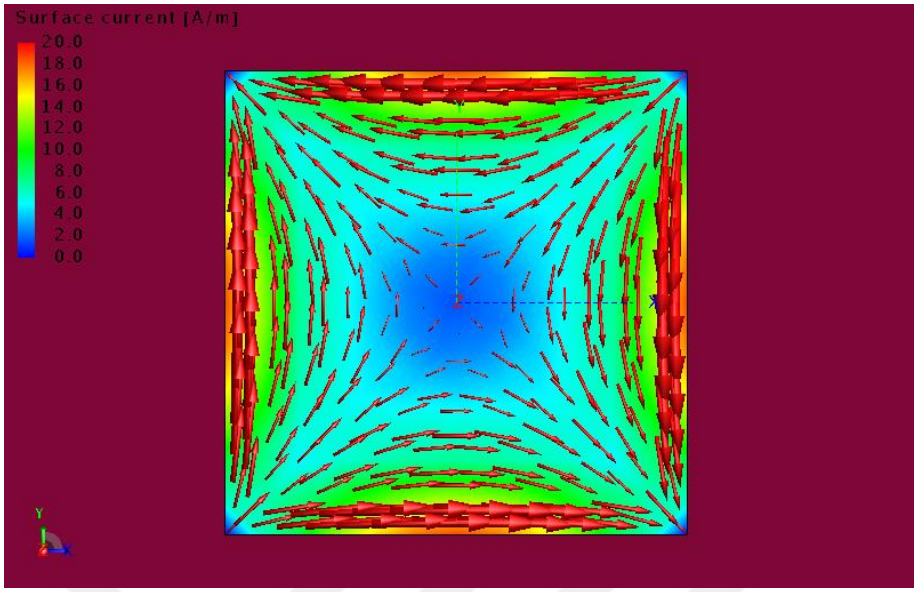

Figure 6. Current distribution of the 3rd eigenmode on square patch at 4.55 GHz

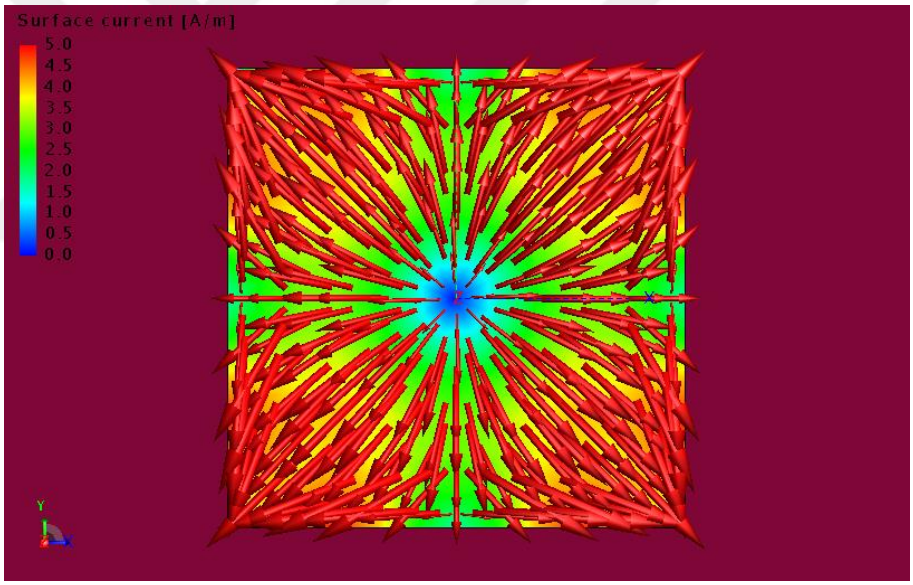

Figure 7. Current distribution of the 4th eigenmode on square patch at 5.85 GHz

As shown in Figure 4 and Figure 5 it is no surprise that the 1st and 2nd modes have identical eigenvalue distribution due to their symmetrical nature, only their polarizations are orthogonal. The 3rd mode on the other hand exhibits a different kind of symmetry along its diagonal and as it will be shown later, this current distribution will be the backbone for the pattern reconfiguration since it will form a tilted main beam. Figure 7 shows the current distribution of another unique orthogonal mode, but as it will be discussed later the pattern formed by this distribution is almost isotropic.

The eigenpatterns of the first four modes are given in Figure 8, Figure 9, Figure 10 and Figure 11, respectively.

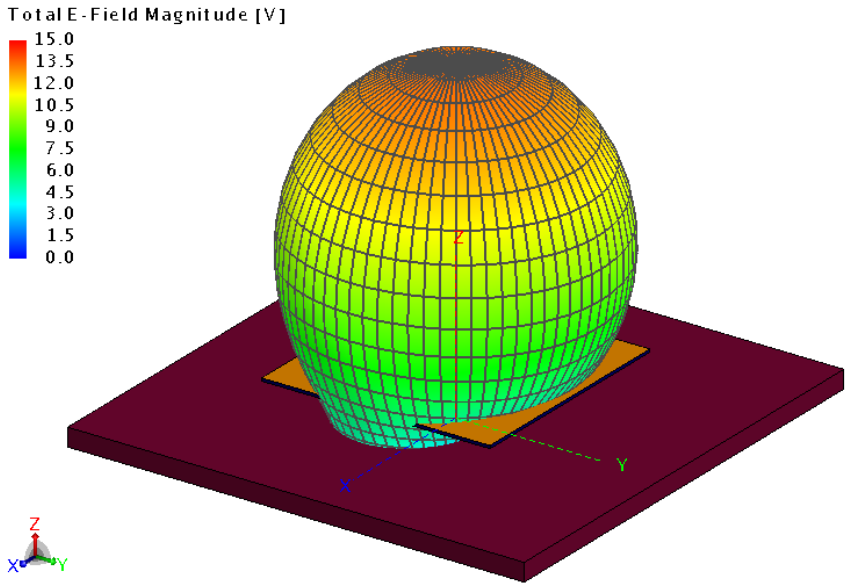

Figure 8. Radiation pattern of the 1st eigenmode on square patch at 3.12 GHz

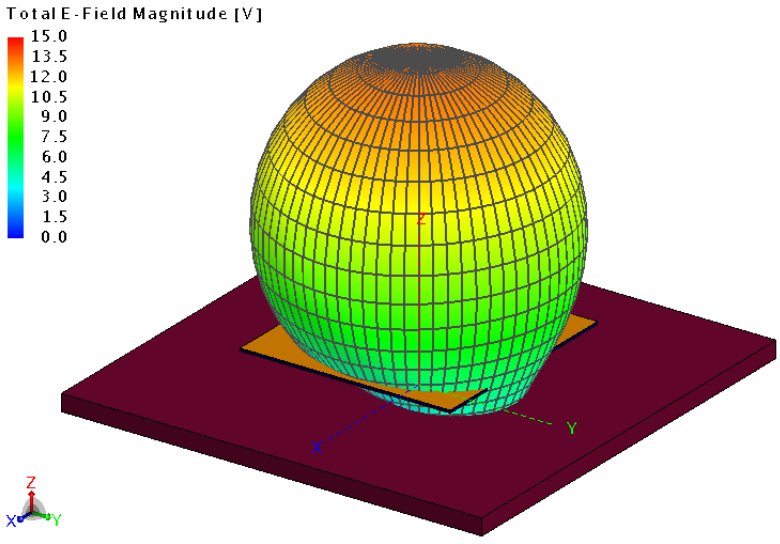

Figure 9. Radiation pattern of the 2nd eigenmode on square patch at 3.12 GHz

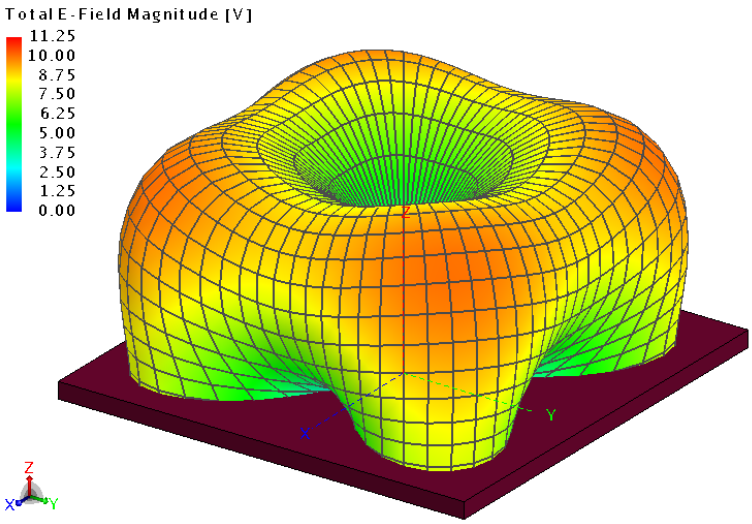

Figure 10. Radiation pattern of the 3rd eigenmode on square patch at 4.55 GHz

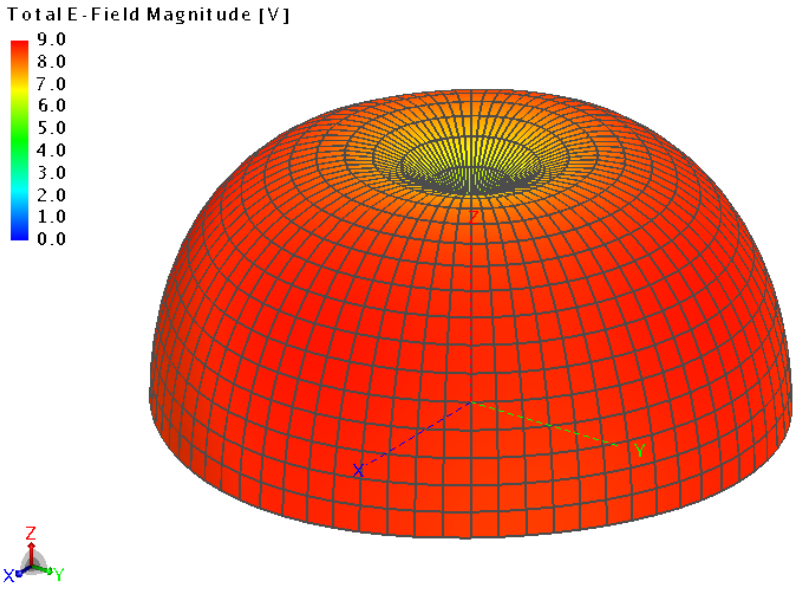

Figure 11. Radiation pattern of the 4th eigenmode on square patch at 5.85 GHz

As expected first two modes resonates at the same frequency, first one with the vertical current distribution, second one with the horizontal current distribution which results in radiation patterns identical at elevation plane and 90^0 rotated with respect to each other in x-y plane. With these first two eigenmodes, some kind of diversity is achieved in azimuth plane, but still the elevation plane pattern remained same. But,

for the third eigenmode a rotation in the elevation plane is also achieved too as it can be seen in Figure 9. First two modes had a broadside beam, but 3rd mode tilts the beam in elevation plane by 37^0. Finally, 4th mode yields an ‘’isotropic’’ kind of pattern which can’t be used as an efficient radiator. So, viable reconfigurable patterns are first three eigenpatterns.

However, one problem remains and that is the resonance frequency of the 3rd mode is far away from the first two modes. From this point on, the goal is to bring the resonance frequencies of these modes closer. To achieve this goal, different type of manipulations will be applied on the shape of the square patch as shown in Table 1. Main motivation during the manipulations is to equalize the electrical lengths travelled by the current vectors for all three eigenmodes. Intuitively, first two modes will resonate at the same frequency as long as the symmetry of the patch is preserved. So, no matter what type of manipulation is done on the patch, keeping the symmetry is a fundamental constraint.

The first thing that can be noticed after checking the current distributions is first two modes have their current concentrated on the edges, but there is still a portion of current flowing through the central area of the patch. However, for the 3rd mode there is almost no current flowing through the central area. 3rd mode almost contains all the current on the edges. This means that if a slot is carved on each edge, the total path travelled by the current vectors for both modes will increase and the resonance frequencies for both modes are expected to get lower values. However, 3rd eigenmode is expected to get even lower resonant frequency since most of the current vectors are confined at the edges for this mode, hopefully this kind of manipulation will reduce the resonant frequency to the resonant frequency of first two eigenmodes.

shows the current distribution for different shaped patches and Table 2 shows the corresponding resonance frequencies along with the 3 dB modal significance bandwidths (i.e. MS>0.707).

Table 1 Characteristic Current Distribution for Different Shaped Patches

Configuration Index	Shape	1st Mode Eigencurrents	3rd Mode Eigencurrents
1	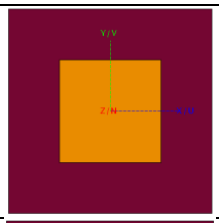	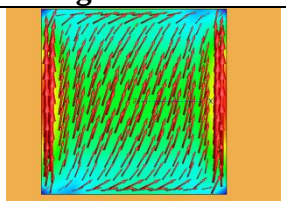	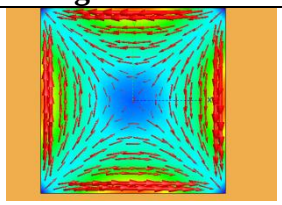
2	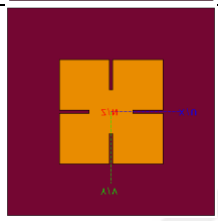	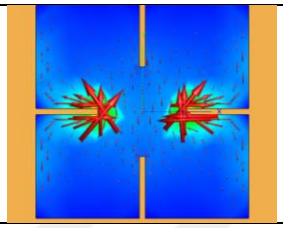	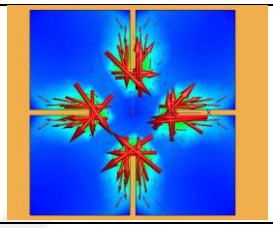
3	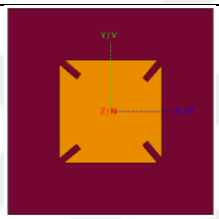	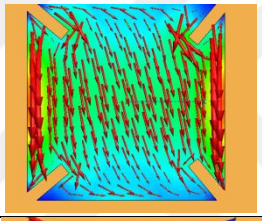	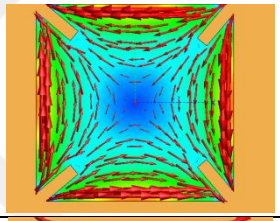
4	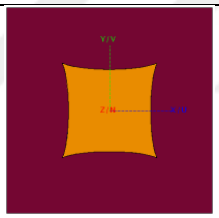	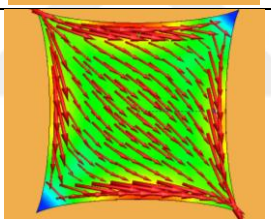	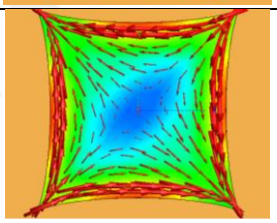
5	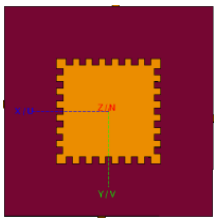	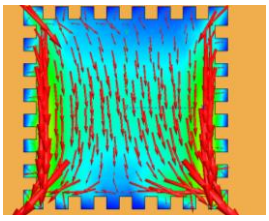	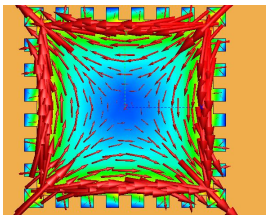
6	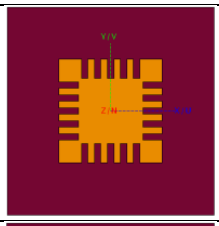	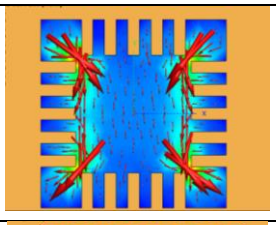	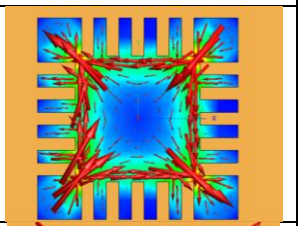
7	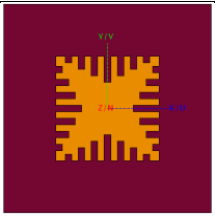	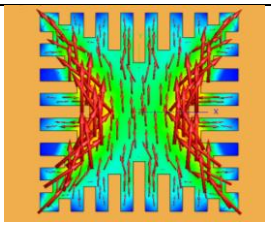	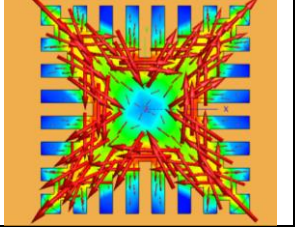

Table 2 Resonance Frequencies and Bandwidths for Different Shaped Patches

Shape	1st and 2nd Eigenmode Resonance Frequency	3rd Eigenmode Resonance Frequency	1st and 2nd Eigenmode Bandwidth	3rd Eigenmode Bandwidth	Frequency Ratio
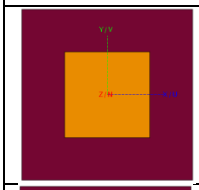	3.12 GHz	4.60 GHz	%14,1	%10,2	1,47
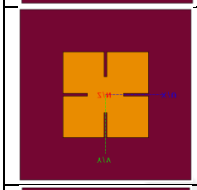	3.10 GHz	4.45 GHz	%12,8	%6,5	1,43
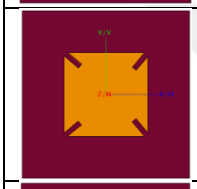	3.05 GHz	4.47 GHz	%9,70	%2,03	1,46
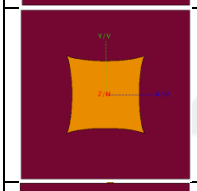	3.54 GHz	5.10 GHz	%13,82	%7,9	1,44
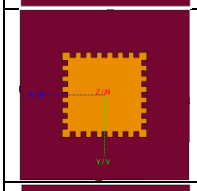	2.72 GHz	3.80 GHz	%5,53	%3,05	1,39
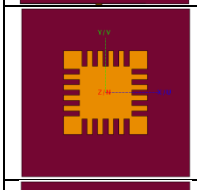	2.71 GHz	3.61 GHz	%5,27	%2,14	1,34
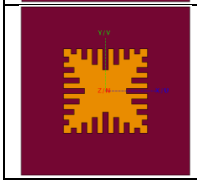	2.74 GHz	3,57 GHz	%4,91	%1,02	1,29

Note that adding single slots as in shape#2 reduced the resonant frequency of 3rd eigenmode from 4.6 GHz to 4.45 GHz, whereas first two resonance frequencies of first two modes reduced from 3.12 GHz to 3.10 GHz. The resonance frequencies got closer, nevertheless they are still too far from each other. The path travelled by the

current vectors need to be increased even further. Also 3 dB bandwidth seems to drop from 10.2% to 6.5% for the 3rd mode.

As it can be seen current vectors at the edges travel $2 * Slot\ Length$ more distance. Unfortunately for single slot the increase in the path length is not sufficient. Different type of slots will be carved till the resonant frequencies get close enough. Shape #3 includes 4 slots on each corner and its resonance frequencies are almost same with the Shape #2 and even worse, the bandwidth is drastically decreased which makes this shape useless as well. Elliptical carves like in Shape #4 prevents the bandwidth to drop dramatically, but they can't provide enough path elongation for current vectors, so resonant frequencies are still far from each other.

To further increase the path travelled for current vectors on edges, multiple rectangular slots are carved on each edge as in shape #5. As it can be seen in Table 2, resonance frequencies got closer more than all the previous cases. However, notice that as the number slots increased, quality factor of the modes increased as well. This situation causes the eigenmodes to have narrower bandwidths. So far it can be inferred that there is a trade-off between quality factor and frequency ratio for these kind of manipulations. This trend can be observed further in shape #6 and shape #7 as well. The current path is dramatically increased and resonance frequencies got very close but bandwidths almost dropped to 1% which makes these modes almost impossible to excite in practice. Even for shape #7, resonance frequencies are still not too close. Unfortunately, the 3rd eigenmode will be investigated at its own resonance frequency from now on. The reason behind being unable to excite them all at the same frequency will be discussed and investigated.

When all the shapes are compared, it seems shape #5 is the most viable solution to make the resonance frequencies close and bandwidth realizable. From now on, this configuration will be used as the antenna element. For this configuration eigenpatterns of the 1st and the 3rd mode are shown in Figure 12 and Figure 13.

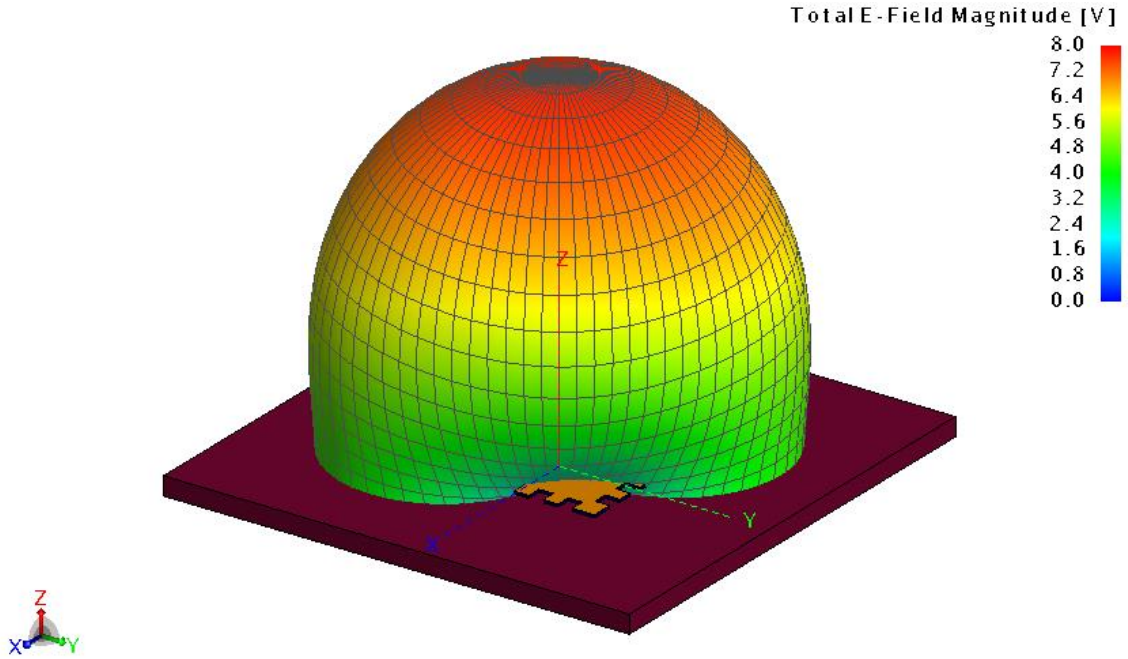

Figure 12. Radiation pattern of the 1st mode on slotted square patch at 2.72 GHz

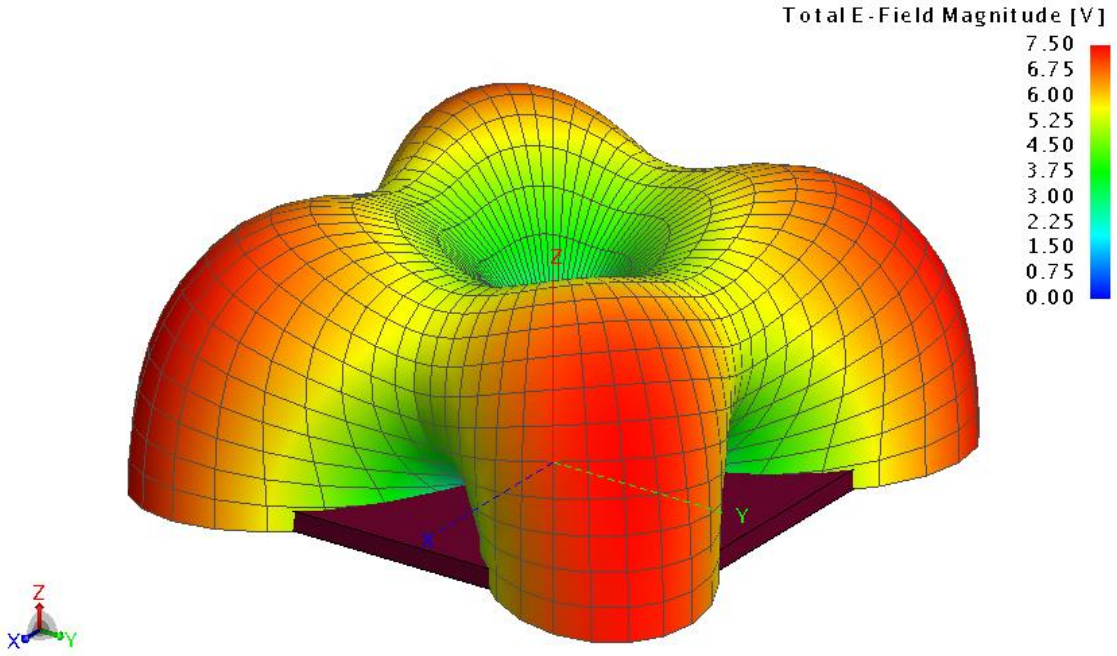

Figure 13. Radiation pattern of the 3rd mode on slotted square patch at 3.80 GHz

When the original and modified radiation patterns are compared, it can be seen that the shape of the patterns are not significantly disturbed, meaning that these modes could still be used for pattern reconfiguration. However, one problem remains and

that is the resonance frequency difference. To make sure whether these two modes can be excited at the same frequency or not the pattern of the 1st mode is checked in the resonance frequency of the 3rd mode. Unfortunately, as shown in Figure 14, characteristic mode analysis of FEKO ceases to track first mode at 3.8 GHz, so the radiation pattern of the first mode could not be obtained at 3.8 GHz. Then, the radiation patterns of the 1st and the 3rd modes are obtained at 3.26 GHz, which is the average of the resonance frequencies of these two modes. The radiation patterns are presented in Figure 15 and Figure 16 for 1st and 3rd modes, respectively. Due to the decreased modal significance values, the scattered E-field magnitude at 3.26 GHz diminishes for both modes. The E-field magnitude of 1st mode is almost halved with respect to its resonance condition and the 3rd mode's E-Field magnitude dropped even more dramatically which turns out to be consistent with the amount of decrease in modal significances. Note that, these scattered E-field magnitudes computed in TCM are only relative values according to some predefined excitations by FEKO. They give an intuition about the radiation efficiency of a particular mode at a certain frequency. These results show that even though the 1st and the 3rd modes could be somehow excited at 3.26 GHz, the realized gain of the element would be poor.

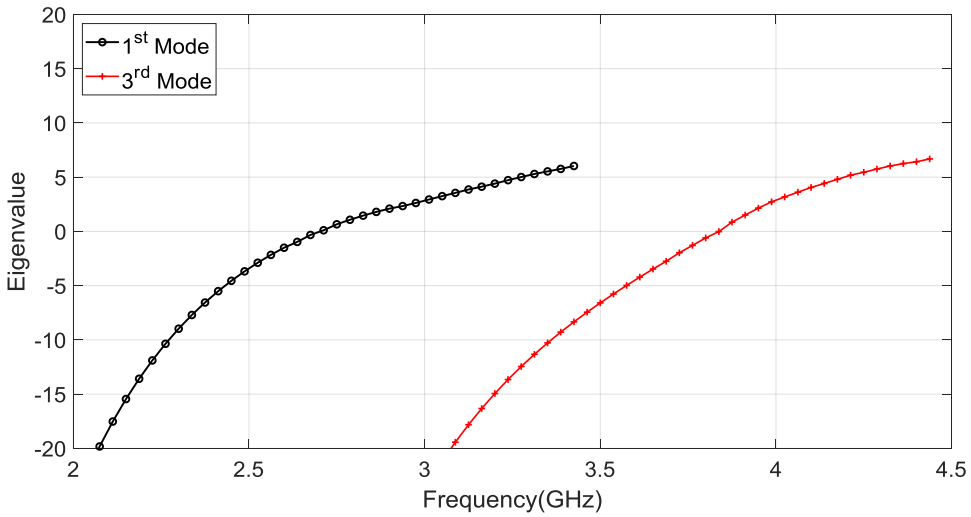

Figure 14. Eigenvalues of the 1st and the 3rd mode on slotted square patch at 3.80 GHz

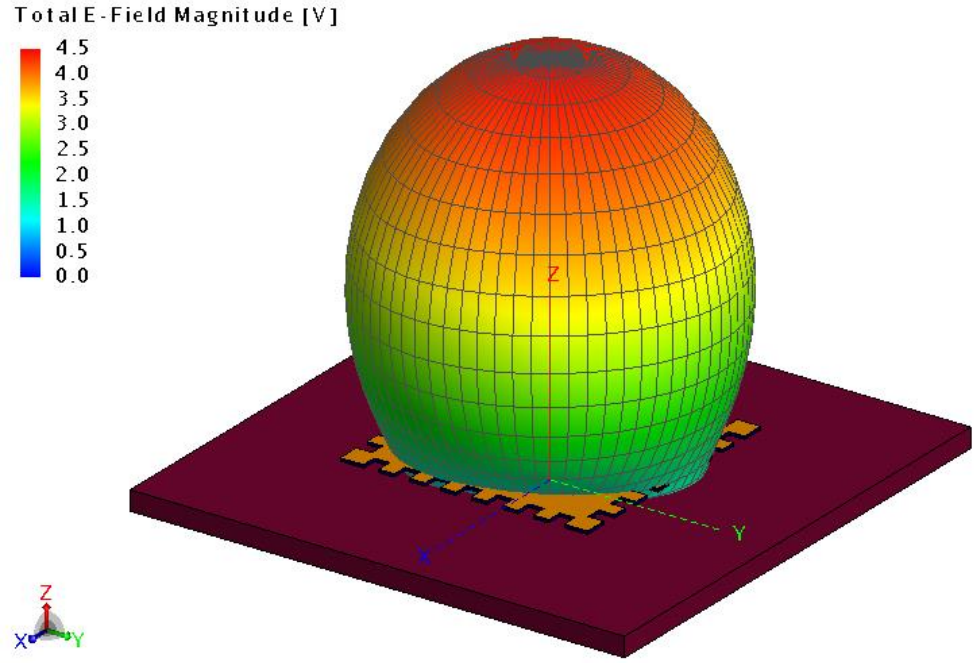

Figure 15. Radiation pattern of the 1st mode at 3.26 GHz

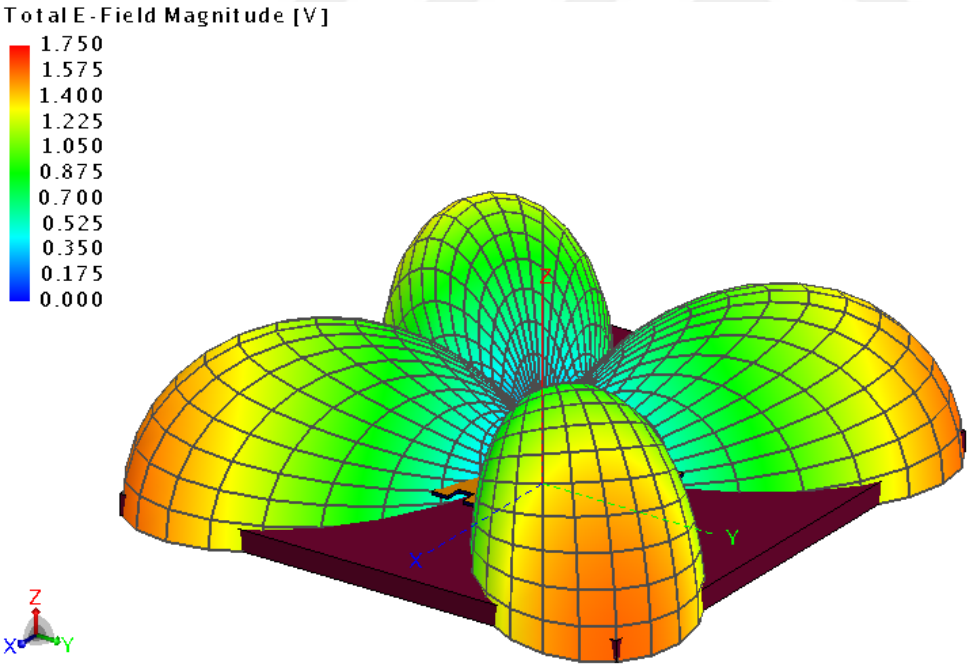

Figure 16. Radiation pattern of the 3rd mode at 3.26 GHz

2.6. Choice of the Feeding Network

As emphasized before in the introduction, feeding network should be small in size, convenient to be fed from a single source and able to distribute the power to multiple elements. Furthermore it should be inexpensive to fabricate, have bandwidth wide enough and suitable to excite different eigenmodes.

Two layer proximity coupled feed topology, which is shown in Figure 17 is chosen since it provides flexibility in choosing dielectric substrates of microstrip patch and microstrip line according to the needs of the corresponding circuit element. For example a substrate with high dielectric constant is generally preferred for microstrip lines so that the fields are more confined beneath the line whereas a substrate with low dielectric constant increases the radiation efficiency and bandwidth of mictrostrip antennas. Therefore the bottom layer dielectric is chosen as RO6010LM [22] whose ϵ_r is 10.7 mm and thickness is 2.4 mm The width of the microstrip line with characteristic impedance of 50 Ω, is calculated to be 2.2 mm.

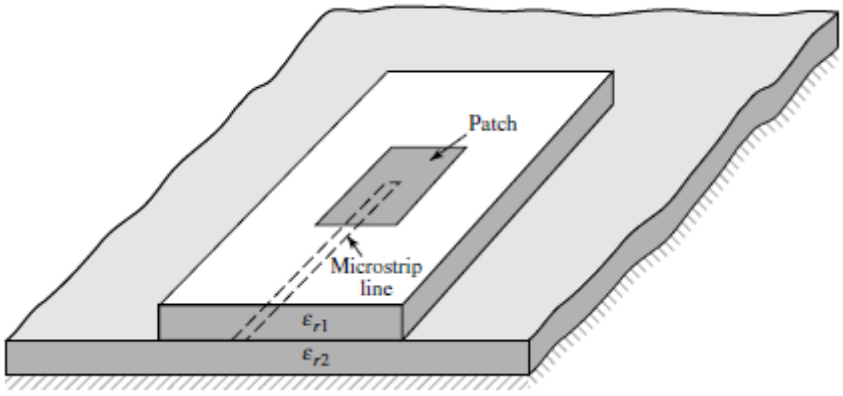

Figure 17. Proximity coupled feed topology [23]

Previously it is mentioned that the MS bandwidth for the 3rd mode becomes narrower when slots are added to the edges. To have a slightly improved bandwidth, 1 mm air gap is inserted between the feeding substrate and the antenna substrate to lower the effective dielectric constant [24]. Nevertheless, the change in the bandwidth was not significant which could be due to the fact that the effective dielectric constant of the antenna is determined by three layers (top dielectric-air-bottom dielectric) and air layer could only compensate the increase in the effective dielectric constant caused by the bottom substrate.

Now that the feeding topology is explained, configurations for different eigenmode excitations will be discussed.

2.7. 1st and 2nd Mode Excitation Schemes

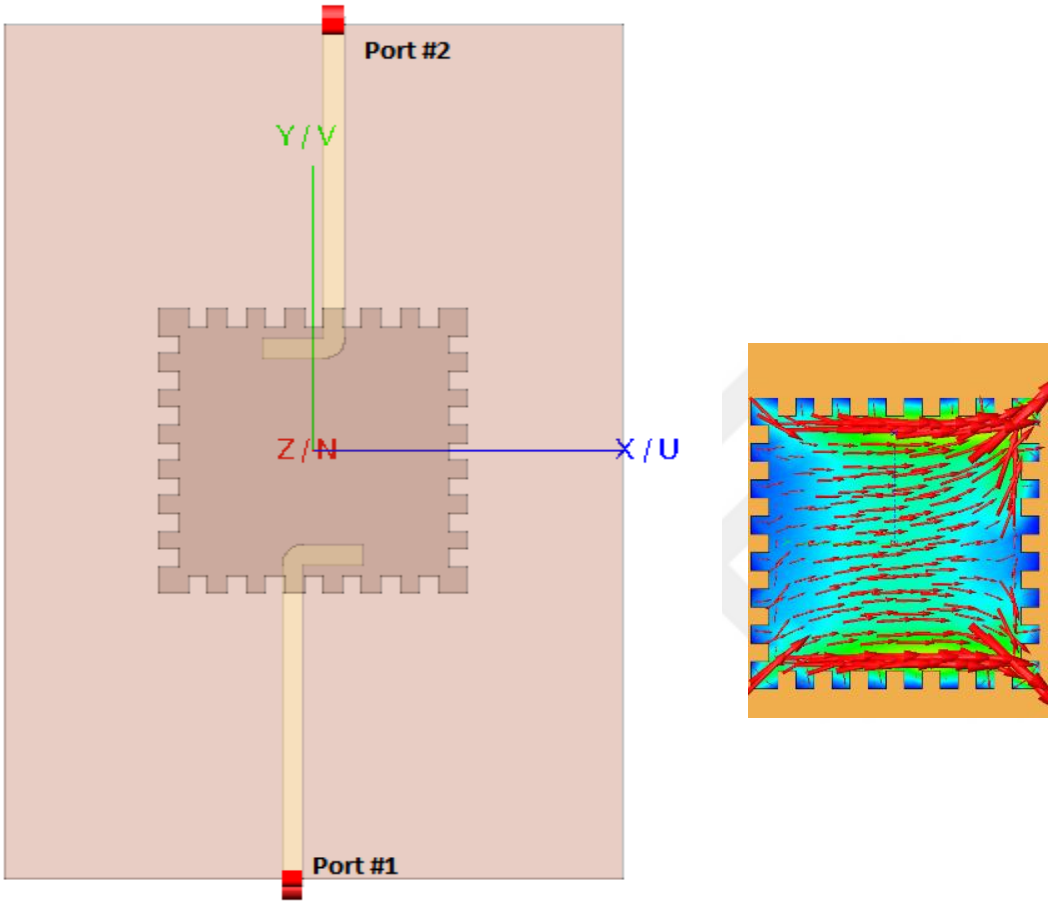

(a) (b)

Figure 18. a) Excitation scheme for the 1st mode, b) Characteristic current of the 1st mode

In order to induce a current distribution similar to the first eigenmode as shown in Figure 18 (b), the patch is fed from opposite sides simultaneously as shown in Figure 18 (a). Note that the current vectors are in the same direction along the edges of the patch for the 1st eigenmode. However, notice that the feeding stubs have opposite orientations. So to compensate this, the 1st and the 2nd ports are fed with 180^0 phase difference.

The length of the microstrip line after the 90^0 bend and the distance between this line segment and the edge of the patch are optimized to minimize the input return loss.

The resulting input return loss and the coupling between these two ports are given in Figure 19.

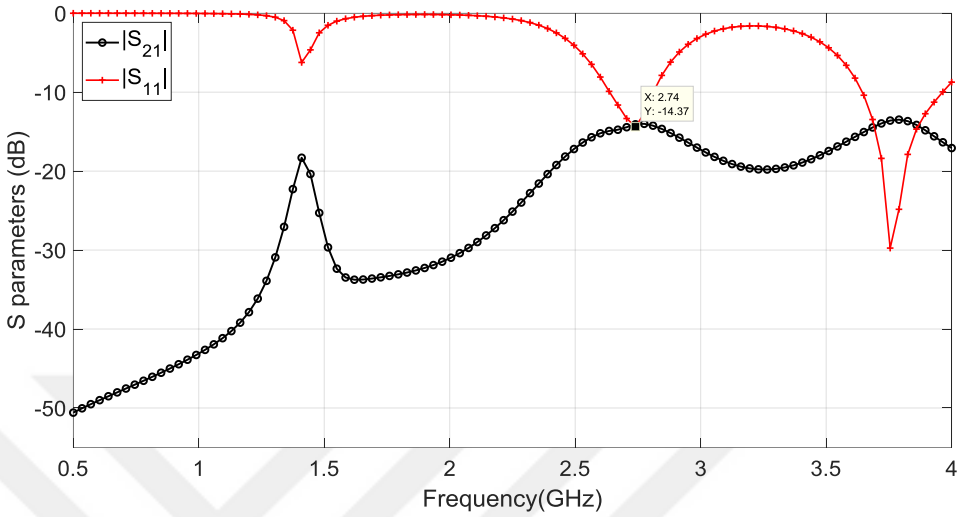

Figure 19. $|s_{11}|$ and $|s_{21}|$ vs. frequency for the 1st mode excitation

According to TCM, the resonance frequencies of the first and the third modes were found as 2.72 GHz and 3.8 GHz, respectively. According to the reflection coefficient results, resonances are observed at 1.4 GHz, 2.74 GHz and 3.75 GHz, which are in agreement with TCM analysis. It can be seen that the coupling between the two feeding ports becomes larger at these resonances, which is expected since the input power from one port could be coupled efficiently to the antenna around these resonance frequencies. The current distribution and the radiation pattern of the antenna are computed at the resonance frequency of the first mode and they are given in Figure 20 and Figure 21, respectively.

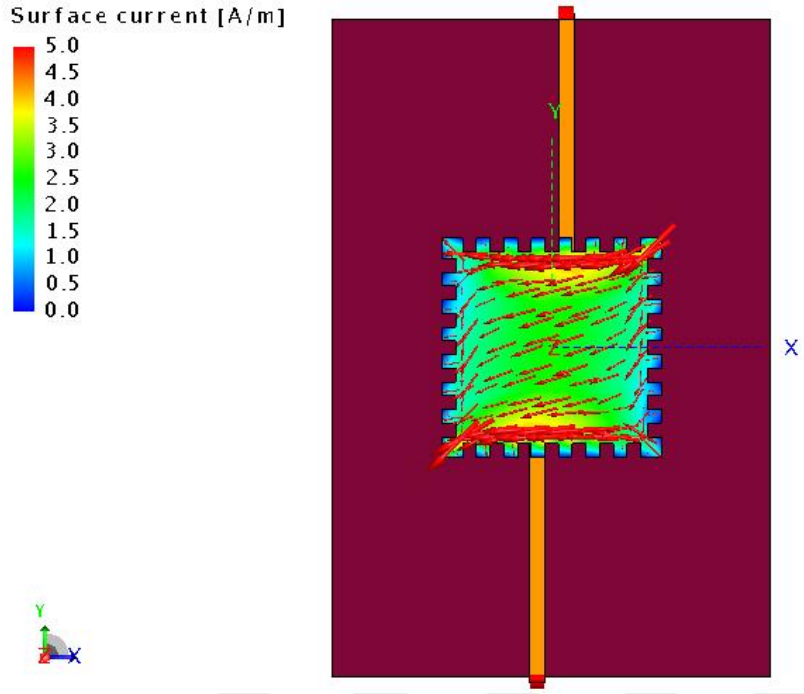

Figure 20. Current distribution for the 1st mode excitation at 2.72 GHz

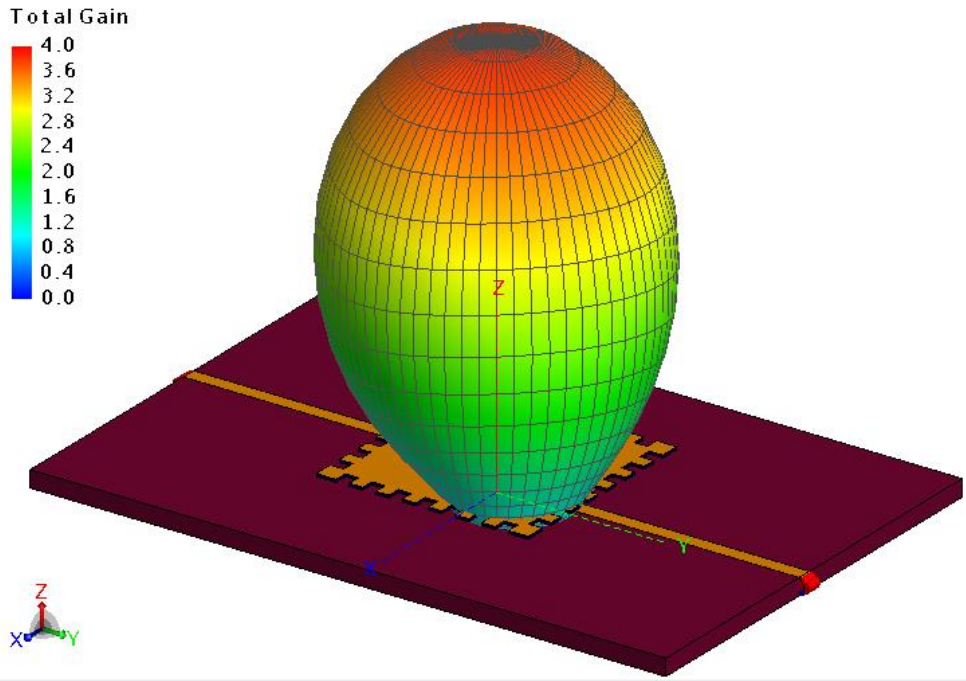

Figure 21. Radiation pattern for the 1st mode excitation at 2.72 GHz

Note that linear scale is used for the entire radiation pattern plots to make the direction of main lobe more visible and distinguishable. It can be concluded that this type of feeding can excite the 1st mode properly with a decent gain of 6 dBi.

Since a low return loss at the resonance frequency of the 3rd mode was observed, the radiation pattern at 3.8 GHz should also be checked and observed whether the 3rd mode is excited simultaneously. In Figure 22 radiation pattern at 3.8 GHz is shown with the same configuration and it can be seen that with this configuration the patch does not behave as an efficient radiator. The pattern does not resemble any of the eigenmodes and it exhibits a poor gain. Hence, having good matching does not necessarily guarantee the antenna to be an effective radiator. Since the coupling between the ports are high at this frequency, probably most of the power fed from one port directly couples to the other port.

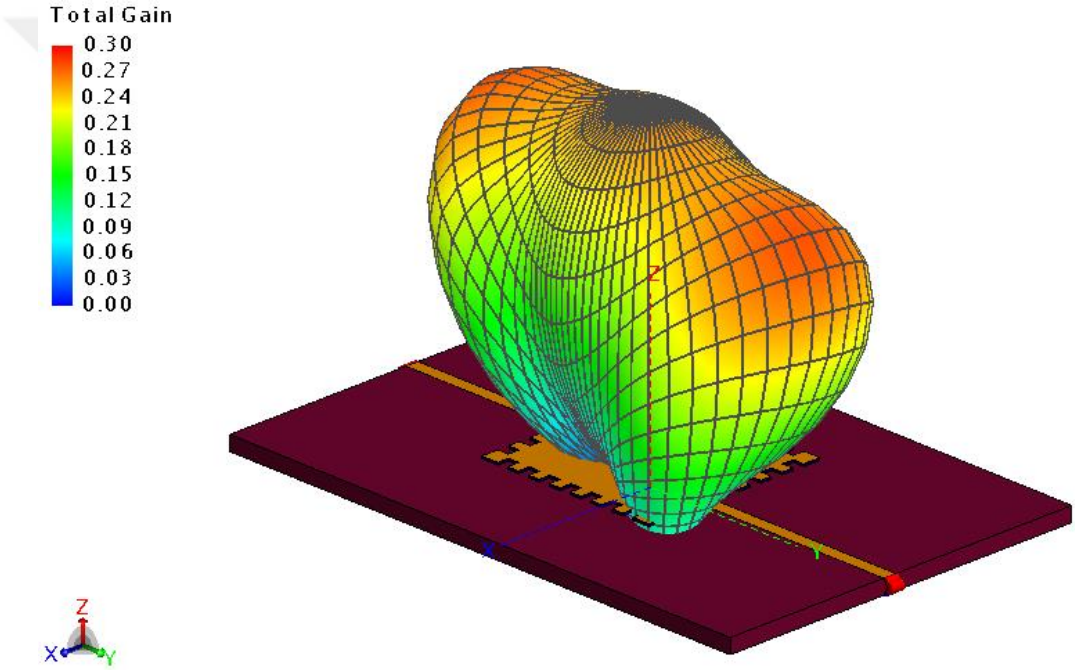

Figure 22. Radiation pattern for the 1st mode excitation at 3.8 GHz

In order to investigate whether a different mode can be excited at 3.8 GHz, where the second resonance is observed, the ports are fed in phase to obtain opposite current directions along the edges. The resultant radiation pattern is presented in Figure 23. There is a null at broadside, and two tilted beams occur in the diagonal plane. It can be observed that by exiting the ports in phase or out of phase two different patterns can be obtained but these two patterns cannot be achieved at the same frequency. The reason might be the high coupling between the ports at resonance frequencies. If the port excitations are adjusted to excite a mode at frequency other than its resonance

frequency, the input power does not couple to the radiating element but it couples to the other port.

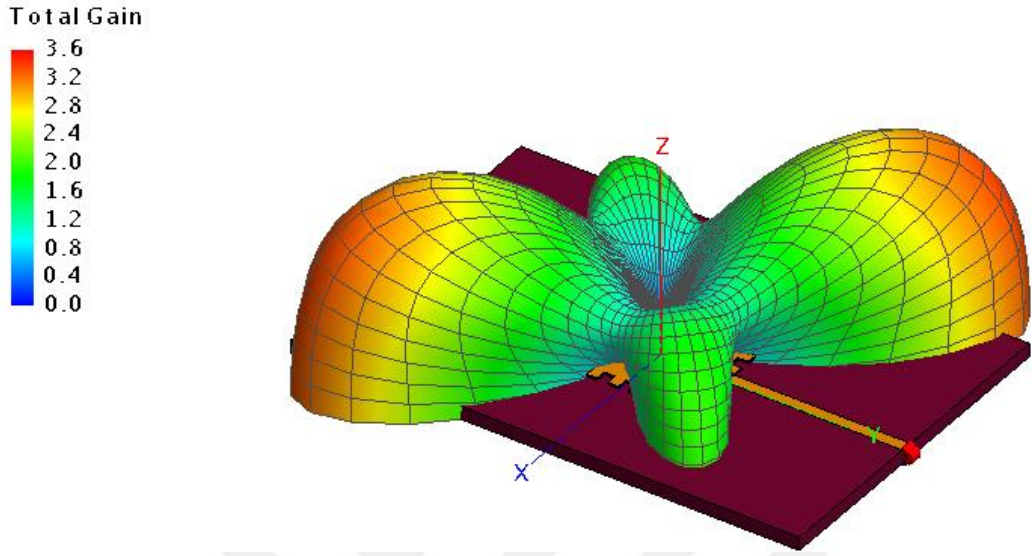

Figure 23. Radiation pattern at 3.8 GHz when ports are fed in phase

2.8 The 3rd Mode Excitation Scheme

Having proposed a feeding topology for the 1st mode, it is time to propose another for the excitation of the 3rd mode. Recall that the current distribution on the patch for the 3rd eigenmode had opposite directions on opposing edges as seen in Figure 24(a). Therefore a four port feeding topology as shown in Figure 24 (b) is used to excite currents on each edge.

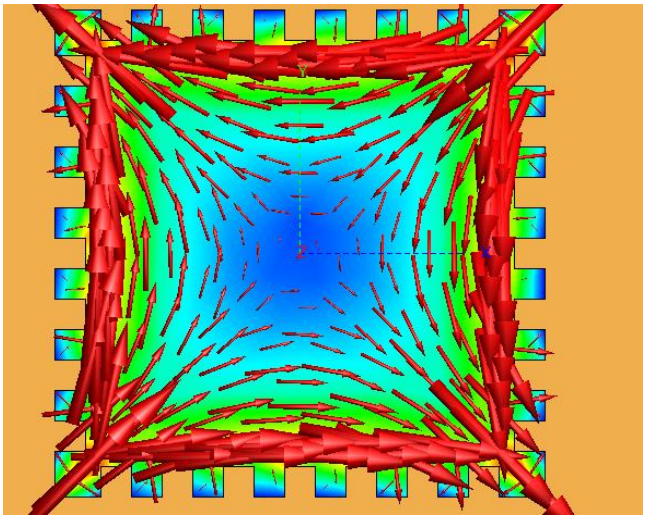

(a)

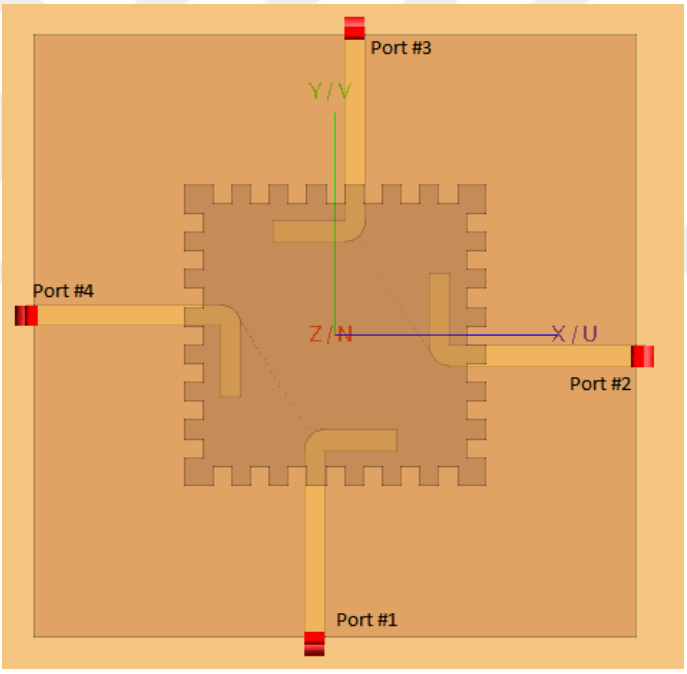

(b)

Figure 24. a) Characteristic current for the 3rd mode, b) Excitation scheme to excite the 3rd mode

When the stub orientations and the direction of characteristic current at the edges are compared it can be seen that, ports 2 and 4 need to be fed with 180 degree phase shift to excite the 3rd mode.

The resulting s-parameters, current distribution and radiation pattern are given in Figure 25, Figure 26 and Figure 27, respectively. Note that for such a configuration there are two different coupling mechanisms. First one is between the adjacent ports and the second one is between the opposing ports which are denoted by S_{21} and S_{31}, respectively. It is interesting to observe that the coupling to the adjacent port increases to high levels at the resonance frequency of the third 3rd mode. This is consistent with the current distribution of the third mode where vertical currents are excited as high as horizontal currents.

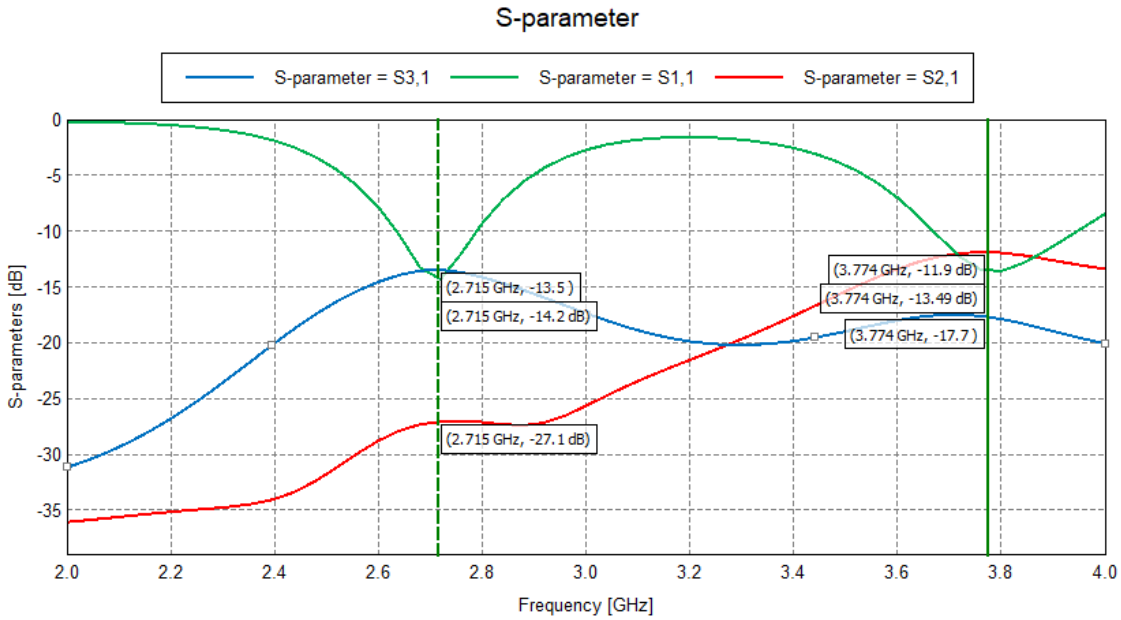

Figure 25. S-parameters versus frequency for 4-port excitation configuration

The current distribution and the radiation pattern plots imply that the third mode can be successfully excited by using the four port configuration.

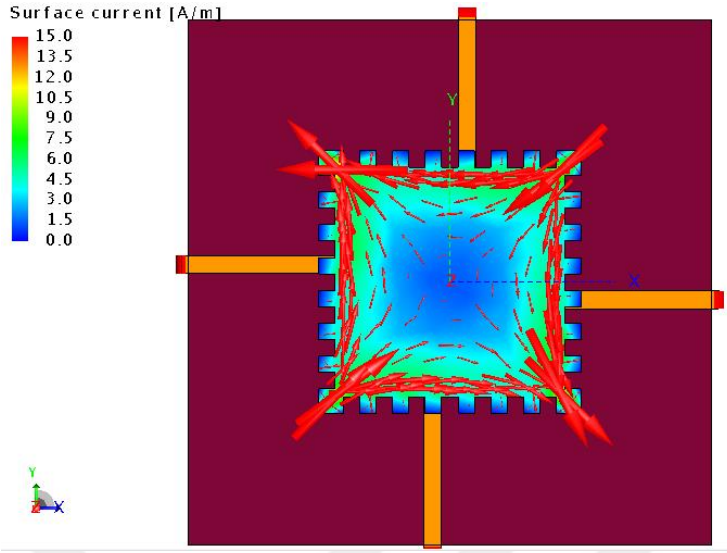

Figure 26. Current distribution at 3.80 GHz with 4-port excitation

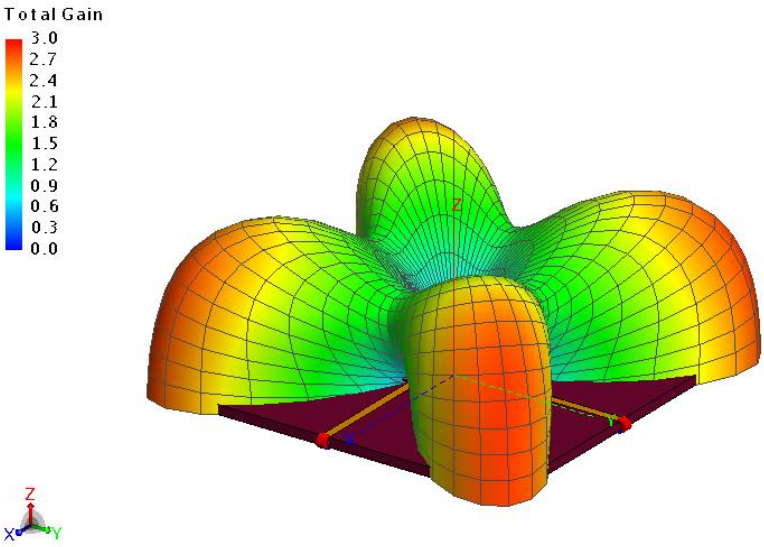

Figure 27. Radiation pattern at 3.80 GHz with 4-port excitation

The 3rd mode's axial ratio values are investigated in Figure 28 to check the type of polarization. The axial ratio takes the value of 100 (20 dB) at the elevation angle of 45 degrees. The gain also takes its maximum value at this angle. So, this result indicates linear polarization for 0^0-180^0-0^0-180^0 feeding scheme.

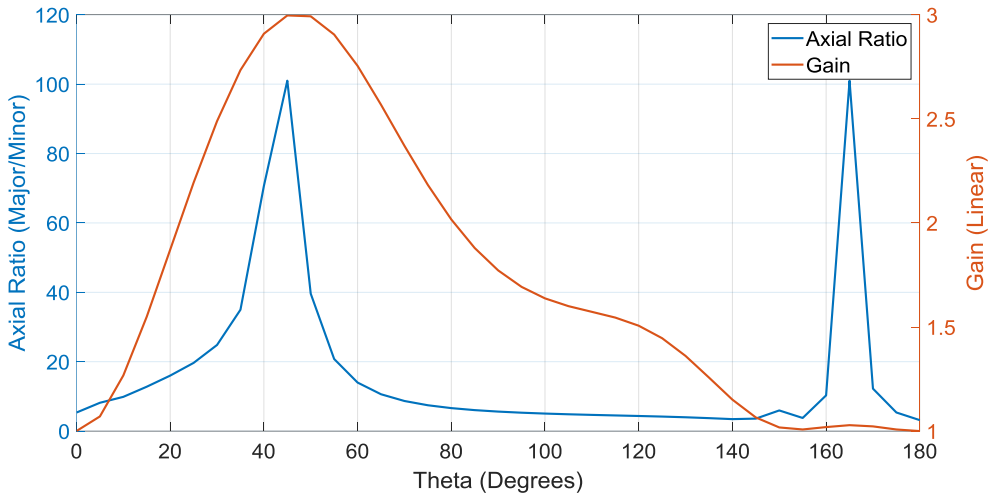

Figure 28: Axial ratio distribution for the 3rd mode excitation

Same configuration is attempted with the phase distribution of 0^0-90^0-0^0-90^0 at ports #1-#2-#3-#4 respectively in order to check if the 3rd mode can be excited in a circularly polarized manner. The resulting current distribution and radiation pattern are presented in Figure 29 and Figure 30. There seems to be an imbalance between the lobes in this case and also the maximum gain is barely 1 dBi. However, the 3 dB decrease in the gain can be explained if one can show the realized polarization type is circular. The axial ratio distribution is given in Figure 31 for this case, although the axial ratio seems to have a relative notch at the maximum gain points it is still above 10 and this prevents to realize a circular polarization. If a completely symmetric feeding structure could be implemented, an ideal circular polarization would be possible.

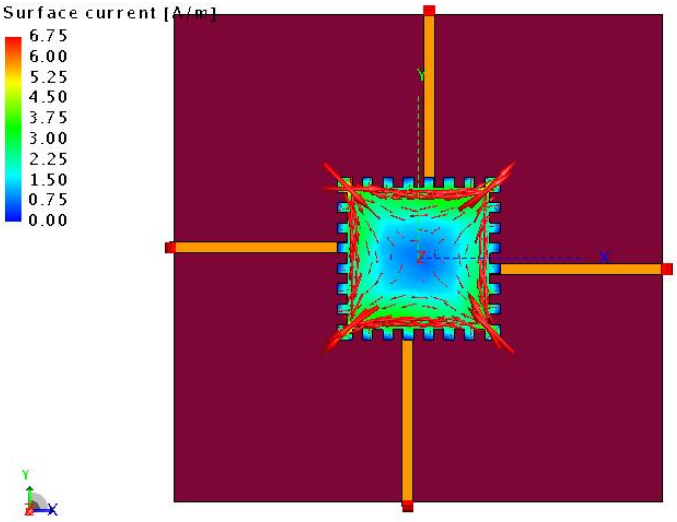

Figure 29. Current distribution at 3.80 GHz with 0^0-90^0-0^0-90^0 4 port excitation

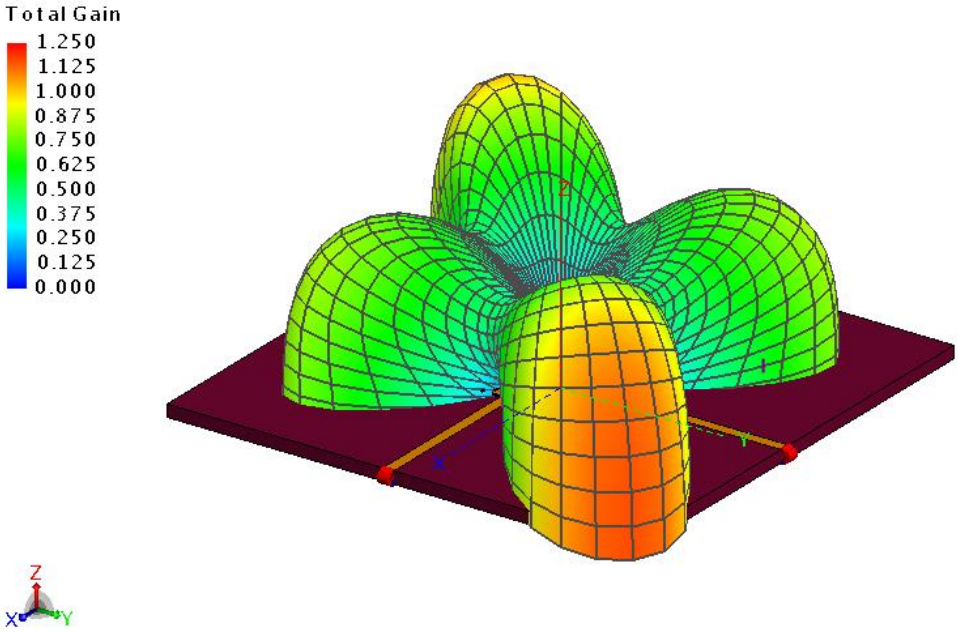

Figure 30. Radiation pattern at 3.80 GHz with 0^0-90^0-0^0-90^0 4 port excitation

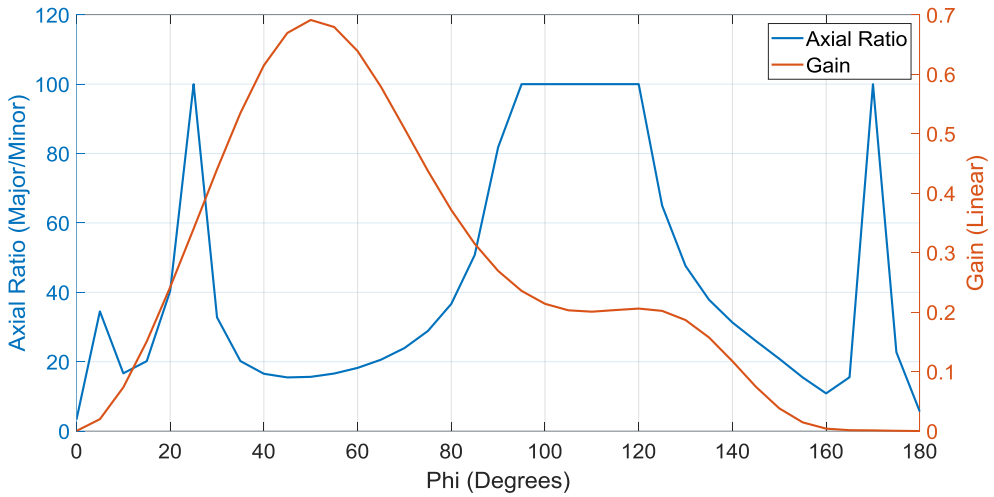

Figure 31: Axial ratio distribution for the 3rd mode excitation with 0^0-90^0-0^0-90^0 feeding configuration

In order to check whether the 1st and the 2nd modes can be excited at 3.8 GHz resonance, Port#1 and Port#2 are fed with 0˚ phase and Port#3 and Port#4 are with 180˚ phase. This phase configuration yields a broadside beam in 2.7 GHz as expected, however the same beam and gain couldn't be achieved at 3.8 GHz due to the interport coupling and poor modal significance as shown in Figure 32 and Figure 33 respectively. Due to this reason these two modes will be excited with these two different feed topologies around their own resonance frequencies.

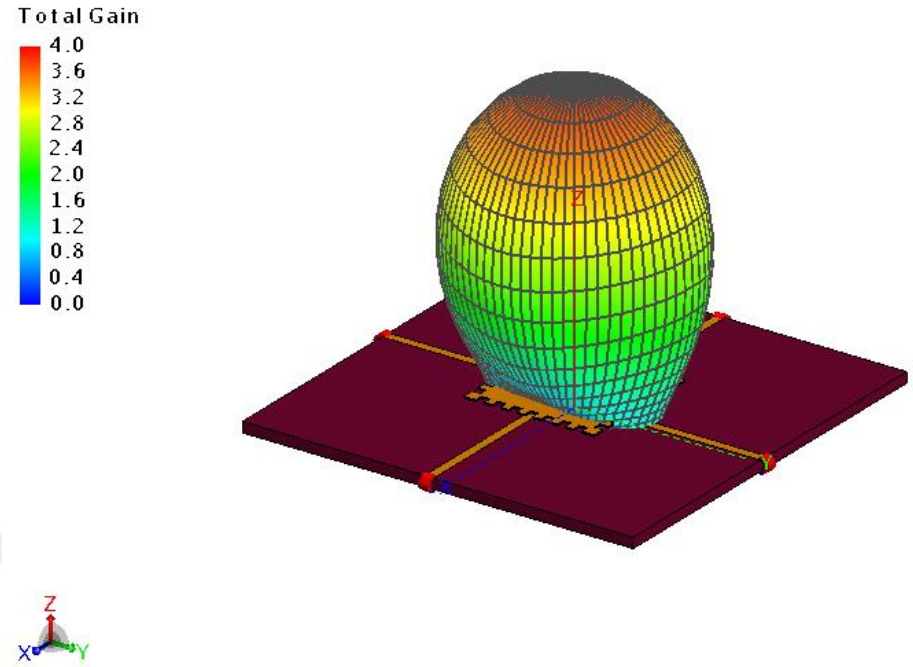

Figure 32. The 1st and the 2nd mode excitation phase configurations at 2.7 GHz

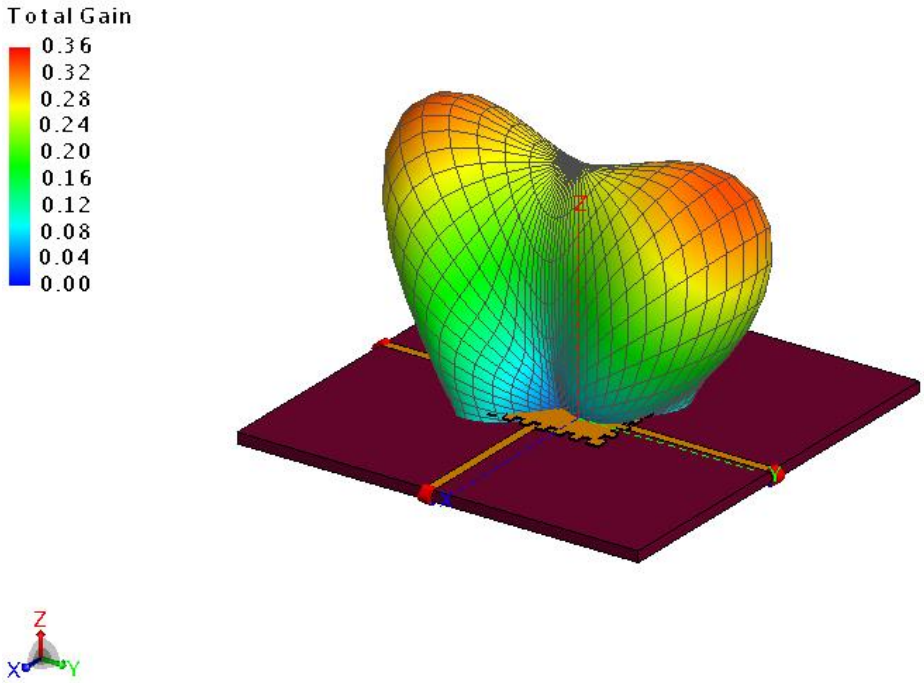

Figure 33. The 1st and the 2nd mode excitation phase configurations at 3.8 GHz

These feeding configurations consists of 90^0 bent stubs, one might ask wouldn't it be possible to realize such a feeding with straight line. As it can be seen in Figure 34, Figure 35 and Figure 36 it is possible. However, return loss S_{11} is not the only

parameter that should be taken into account during the design since couplings between the ports should also be minimized. If the couplings between adjacent ports are compared for both configurations, it can be seen in Figure 24 that straight lines yield higher coupling (-10 dB at resonance) although the gain and return loss values satisfy the modal properties. Bent stubs on the other hand satisfy -13 dB coupling between adjacent ports.

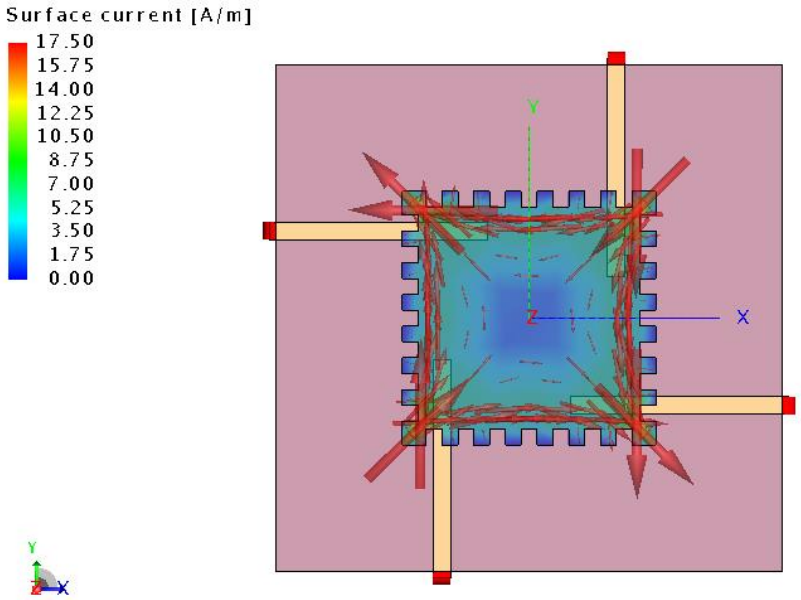

Figure 34. Current distribution for the 3rd mode excitation at 3.80 GHz with straight feeds

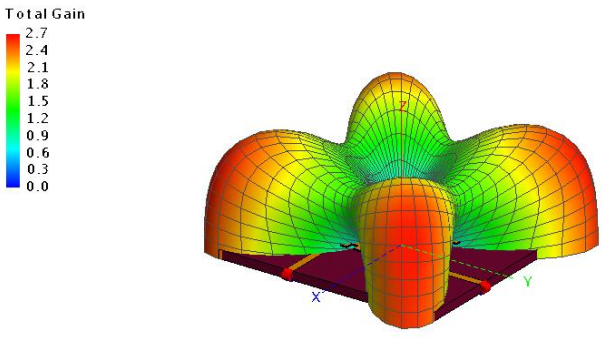

Figure 35. Radiation pattern for the 3rd mode excitation at 3.80 GHz with straight feeds

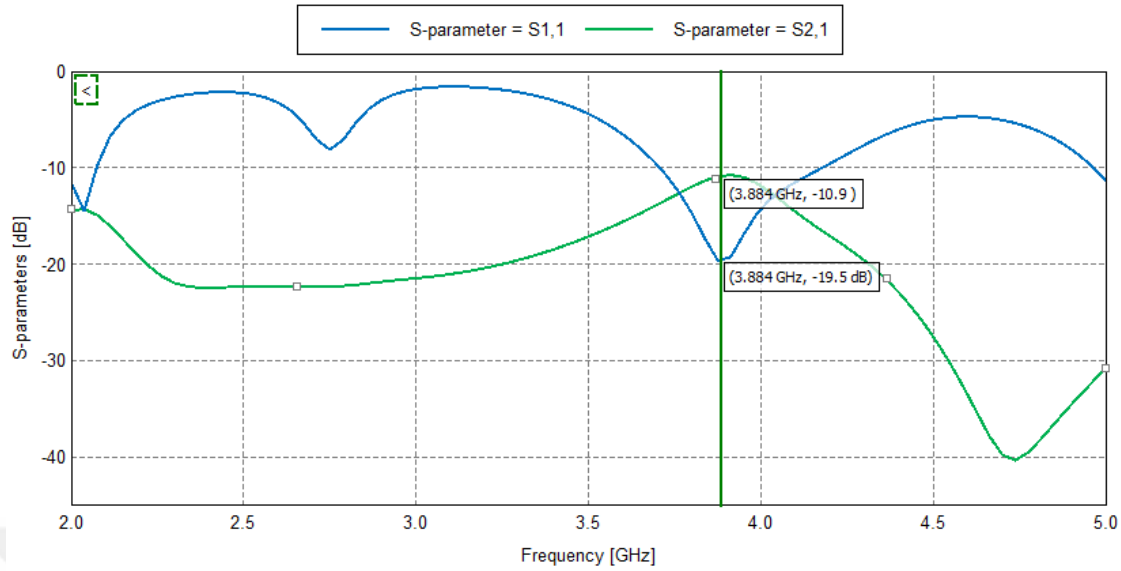

Figure 36. S-parameters for straight line feeding scheme

2.9. The 1st and the 2nd Mode Excitation from a Single Port Using T-junctions

In the previous section each side of the patch is excited by a separate port. Doing so makes it simple to excite the desired eigenmode since phase of the sources at each port can be set by choice. However, the ultimate goal is to achieve the desired excitation by utilizing a single feeding network with a single port. To do so, input power should be equally divided among each feeding branch. Moreover, the phase difference between the end points of each feeding branch should be adjusted accordingly for each mode as stated in previous chapter. Note that, single port excitation does not mean that only one feeding branch will be used. The number of feeding branches, their relative amplitudes and phase differences will remain same with the previously mentioned schemes. It means that these branches will be fed from a single source and all the power division and phase adjustments will be done on a suitable network for each mode as it will be explained later.

One can achieve this type of power division in using different techniques. There are different types of solutions for a variety of applications such as branch line couplers, ratrace couplers, Wilkinson power dividers, T-junction and so on. T-junctions will be proposed for this application due to their ease of implementation, although there are

some drawbacks such as slightly higher return losses, higher interbranch coupling and higher transmission losses due to increased line lengths. In later parts same configurations realized with the ratrace couplers and simulation results are observed and comparisons with the T-junctions are made.

Figure 37 shows the feeding configuration for first two modes when a T-junction is used as a power divider. As it can be seen in Figure 37, in order to have the exact 180^0 phase difference at the end of the feed points, line lengths of each branch are optimized. The main drawback was the amplitude fluctuations due to the non-symmetrical structure of the feed lines.

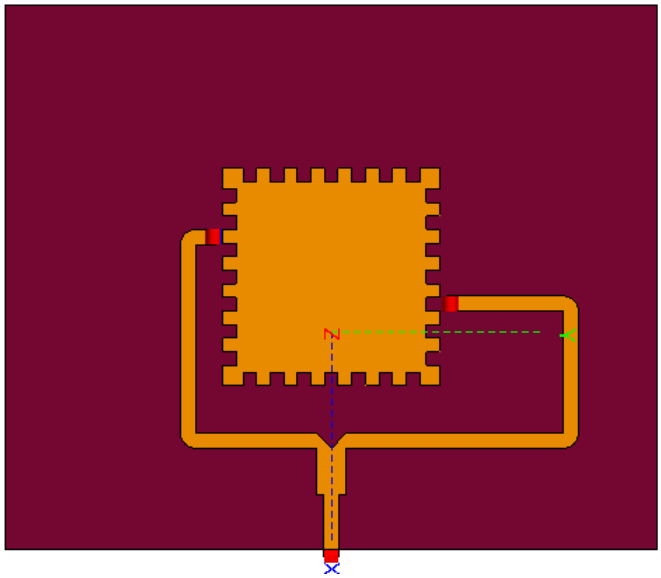

Figure 37. T-junction feeding scheme for the 1st mode excitation

Figure 38 and Figure 39 show the magnitude and phase of s-parameters for the T-junction where port 1 is the input port, port 2 and port 3 are the output ports. At the resonance frequency of the first mode (2.72 GHz) magnitude difference between two output ports is approximately 0.3 dB mainly due to the line length differences and phase difference is exactly 180^0. Return loss is below -12 dB around the resonance frequency. These results indicate that such a topology can be legitimately used to excite the 1st mode.

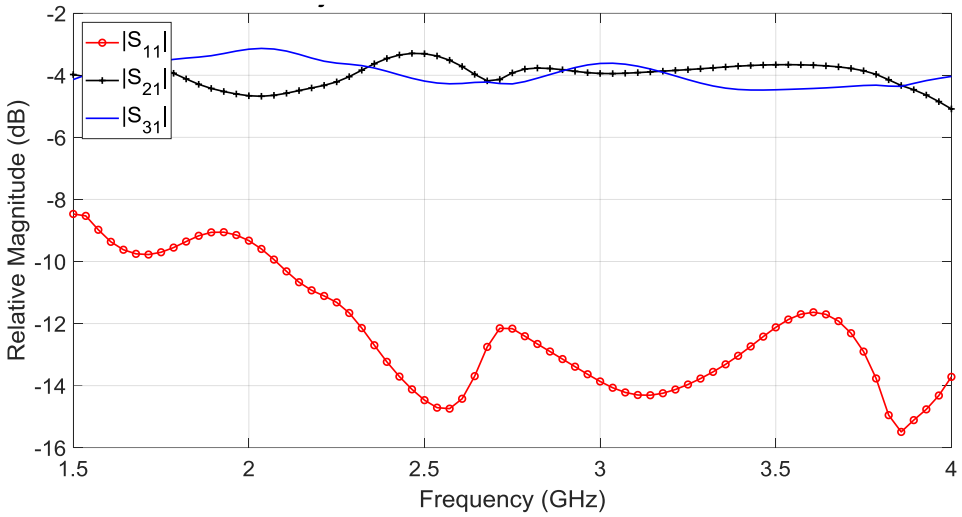

Figure 38. S parameters vs. frequency for the T-junction

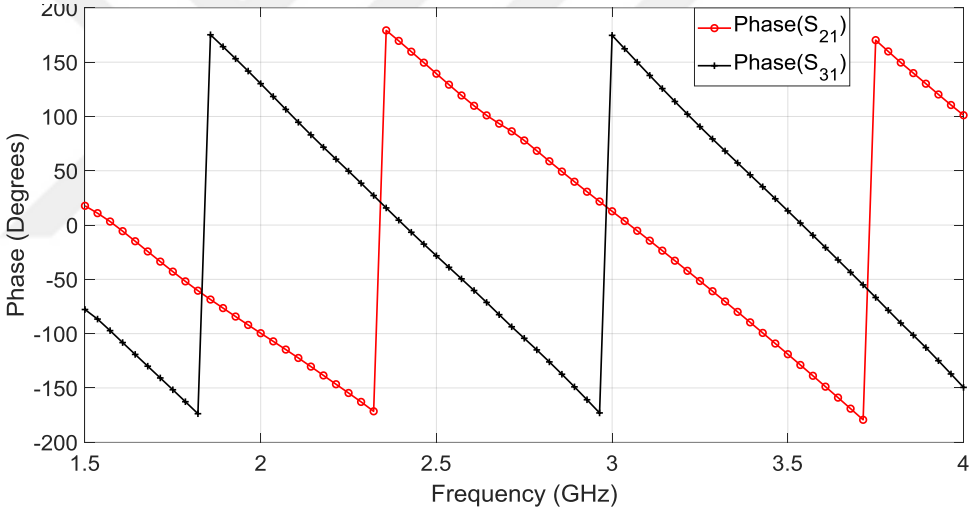

Figure 39. Phase distribution vs. frequency for the 1st mode excitation with T-junction

After ensuring the equal amplitude and out of phase feedings, the stubs beneath the patch can be placed whose lengths and positions were optimized earlier. Then, the resulting current distributions and radiation pattern of the antenna can be observed in Figure 40 and Figure 41, respectively. Figure 40 indicates the 1st mode is successfully excited, moreover 6 dBi realised gain shown in Figure 41 demonstrates how efficiently the patch radiates at broadside as expected.

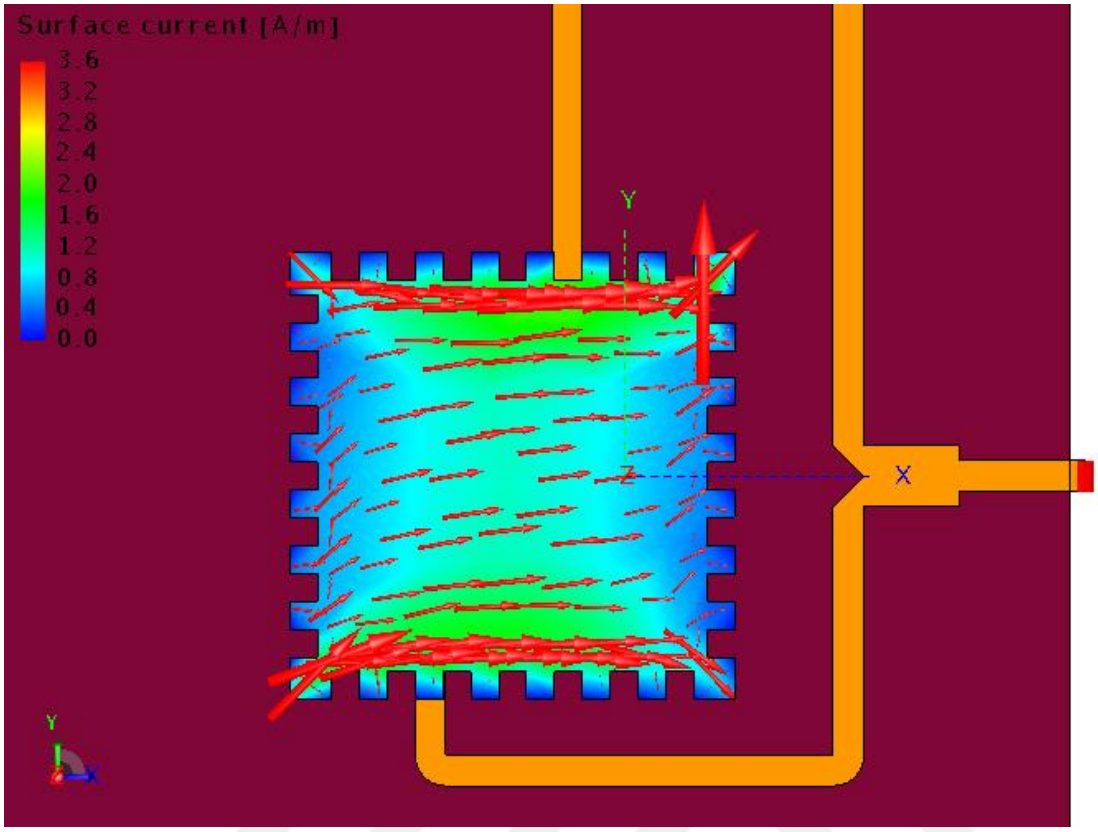

Figure 40. Current distribution for the 1st mode excitation with T-junction feeding

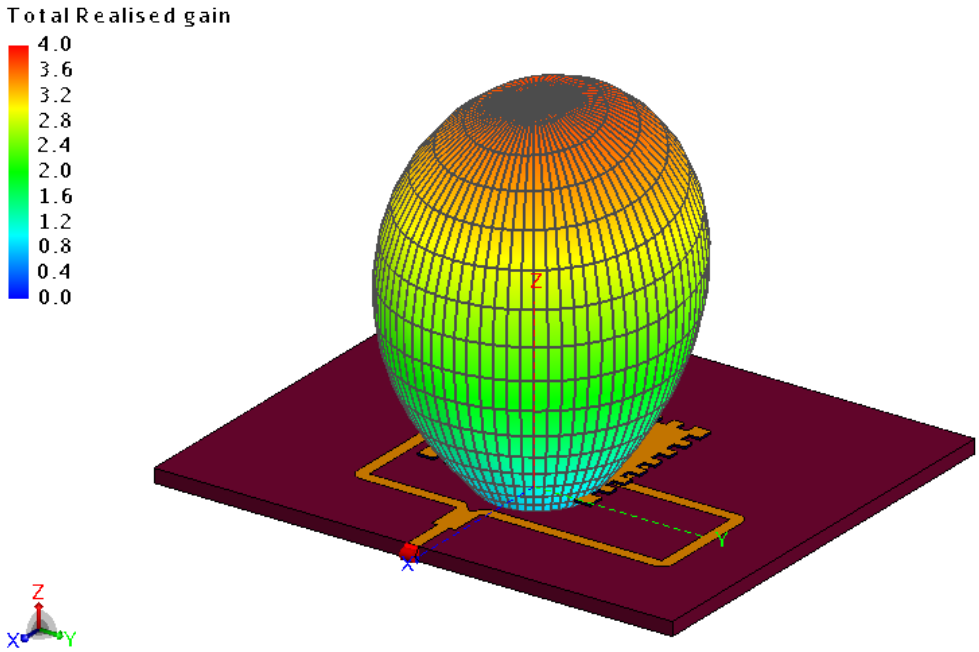

Figure 41. Radiation pattern for the 1st mode excitation with T-junction feeding

Figure 48 shows the matching requirement is also satisfied as S_{11} is below -10 dB at resonance frequency with a bandwidth of 7%.

2.10. The 3rd Mode Excitation from a Single Port Using T-junctions

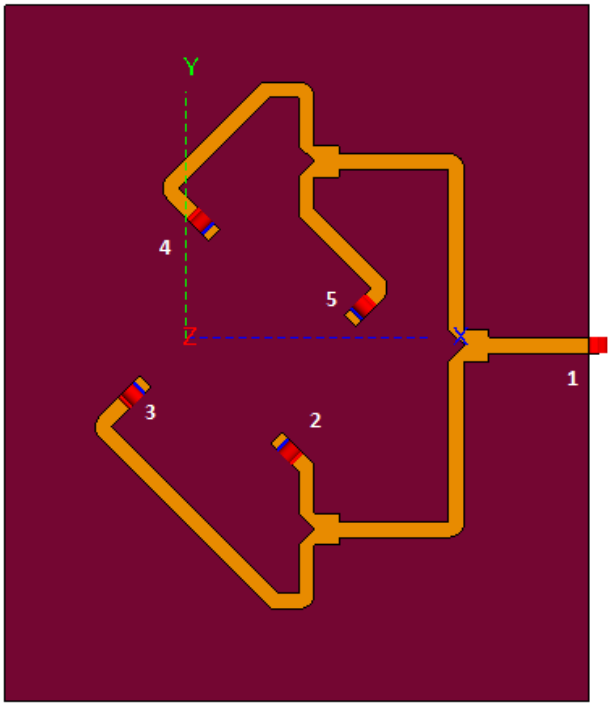

Figure 42. T-junction Feeding Scheme for the 3rd mode excitation

The same technique of equal power division and appropriate phase distribution is obtained for the 3rd mode by using three T-junctions as shown in Figure 42. In order to have the phase distribution of 0^0-180^0-0^0-180^0 at the ports #2-#3-#4-#5, respectively, the length adjustments are implemented at the branches of the secondary T-junctions. The first T-junction has completely symmetric branches in order to keep phase and magnitudes uniform at the input of the secondary T-junctions.

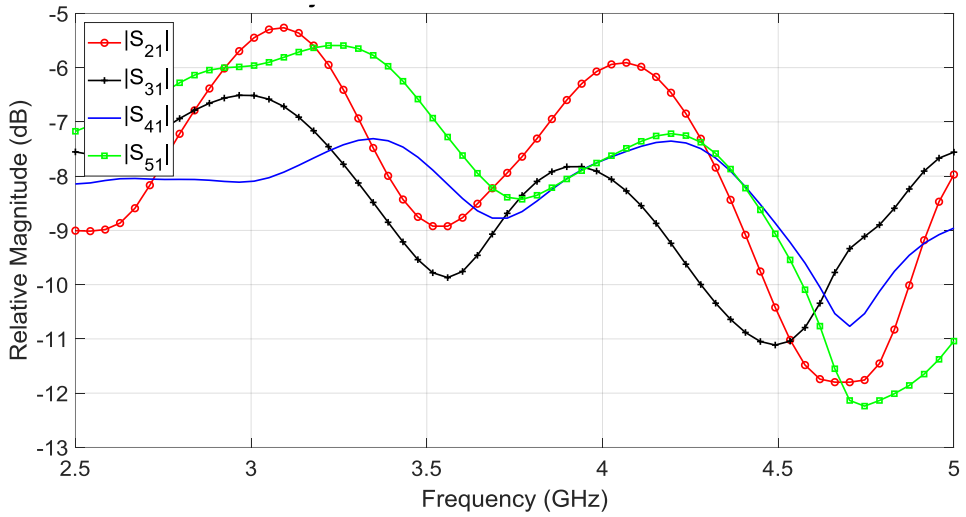

Figure 43. S parameters vs. frequency for the 1st mode excitation with T-junction

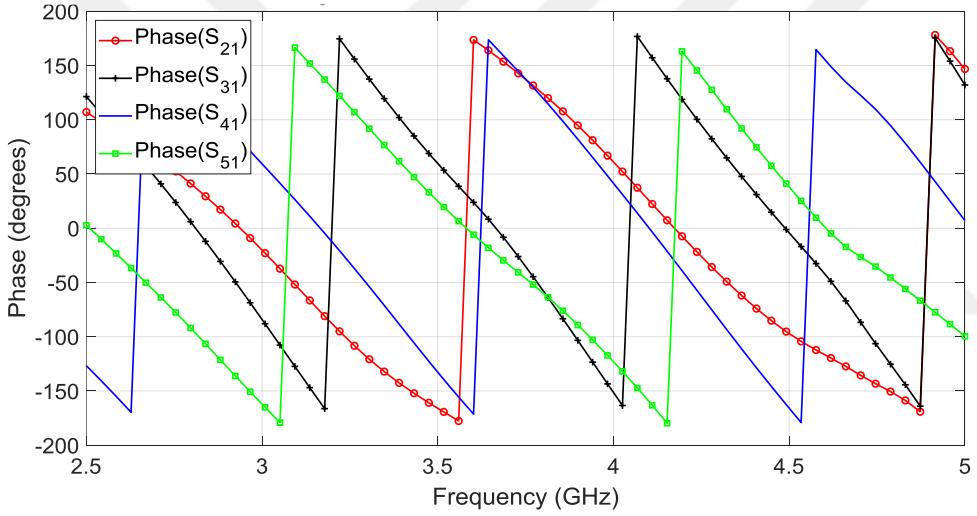

Figure 44. Phase distribution vs. frequency for the 3rd mode excitation with T-junction

As the number of branches is doubled, it became more difficult to both adjust the phases at the end points and equalize the magnitudes. The worst case magnitude difference between the ports #2 and #4 is 0.6 dB as seen in Figure 43 , furthermore a phase error of 5^0 occurs between the ports #2 and #4 as shown in Figure 44. Nevertheless, desired current distribution and radiation patterns are obtained for the 3rd mode as illustrated in Figure 45 and Figure 46. One discrepancy between the 3rd mode's radiation pattern and the pattern obtained after the feeding can be observed though. All of the four main beams should have had the symmetric characteristics, but figure 40 indicates an imbalance between the beams, namely the beams directed along the Y-Z plane exhibit 4.7 dBi gain whereas the beams directed along X-Z plane exhibit

4 dBi gain. This is actually due to phase and magnitude errors discussed above. This also reminds the vital importance of equal magnitude requirement for the feed ends.

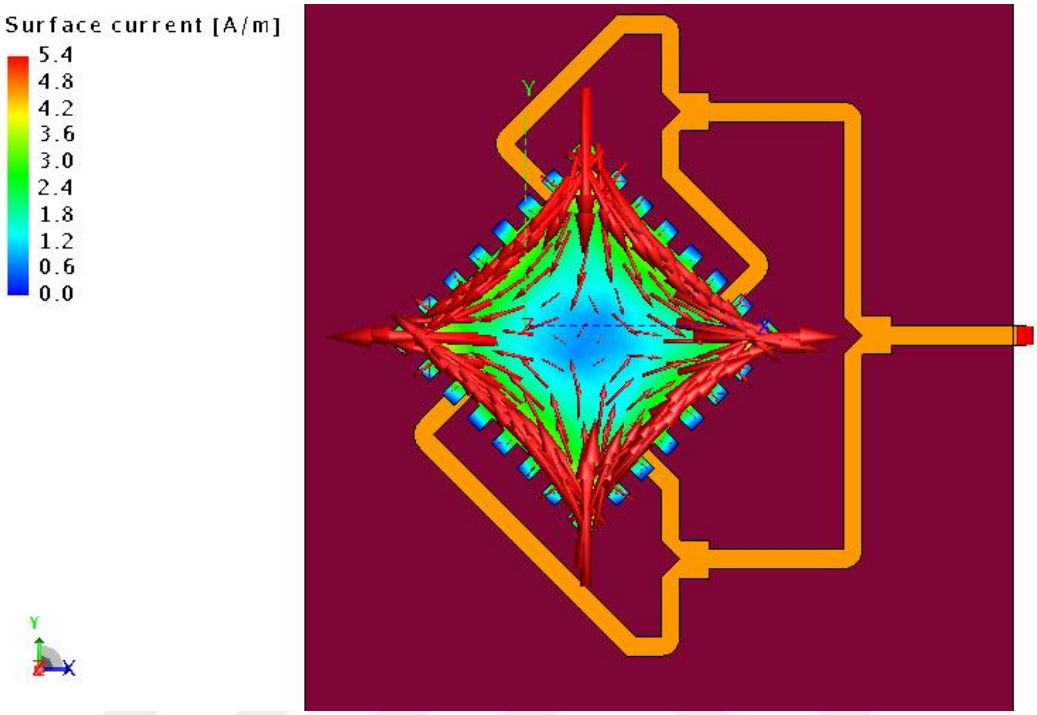

Figure 45. Current distribution for the 3rd mode excitation with T-junction feeding

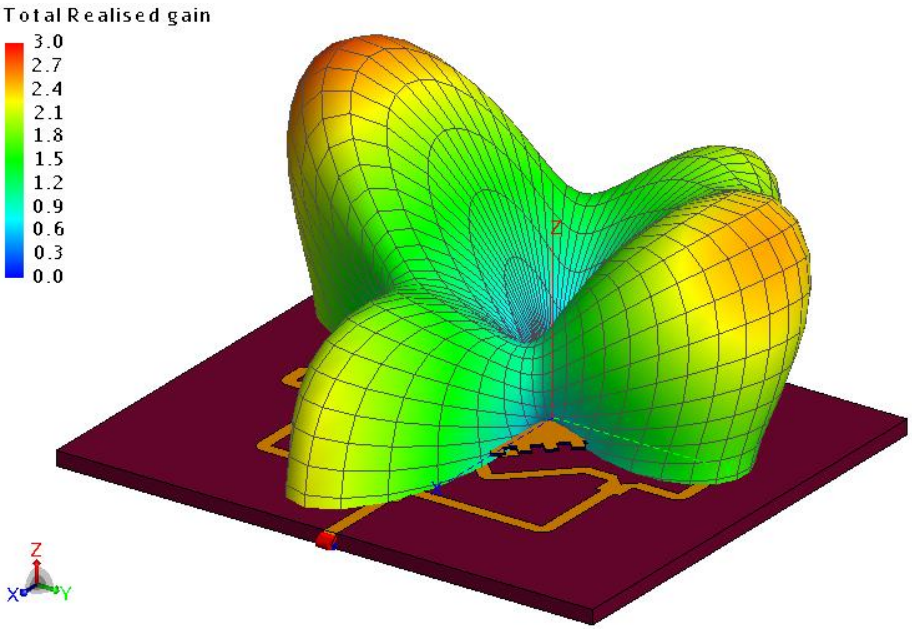

Figure 46. Radiation pattern for the 3rd mode excitation with T-junction feeding

CHAPTER 3

MEASUREMENT RESULTS

3.1. S-parameter Measurements

The realized structure looks like in Figure 47 for the excitation of the 1st mode. Both the slotted patch and the feeding structures are fabricated by LPKF ProtoMat S100 [25]. Eagle Autodesk software [26] is used for creating the necessary gerber files. Keysight Agilent N5230A [27] Vector Network Analyzer (VNA) is used for measuring S_{11}. VNA results and simulated results are compared in Figure 48. When realizing the feed lines for the 1st mode, copper is etched a little bit deeper than expected, in order to compensate those tiny gaps some solder is melted in the gaps as it can be seen in Figure 47.

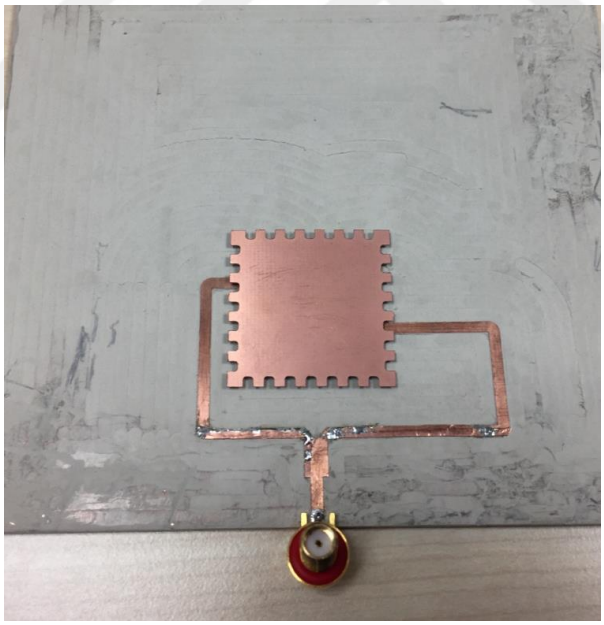

Figure 47. Realized structure for the 1st mode excitation with T-junction

In order to feed the structure edge mount SMA connector from Amphenol [28] is soldered on the edge of feed substrate.

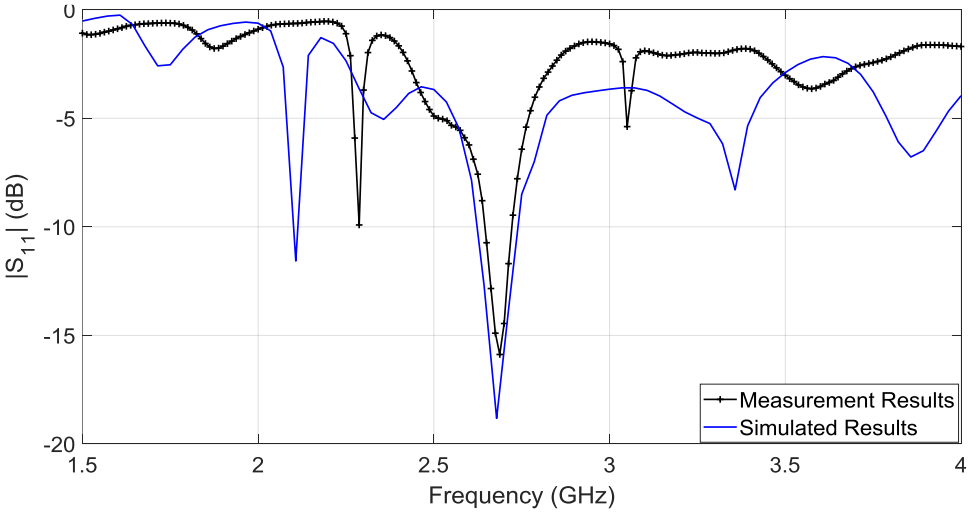

Figure 48. S_{11} vs. frequency of realized structure for the 1st mode excitation

As it is seen in Figure 48, the 1st eigenmode resonance frequency is very close in both measurements and simulation. The behavior of S_{11} is also similar for out of resonance band. The only small discrepancy here seems the bandwidths. Bandwidth of measured antenna seems 1% narrower which can be explained by non-ideal processes during the fabrication such as the feed line defects, connector losses and material tolerances.

The realized structure looks like in Figure 49 for the excitation of the 3rd mode.

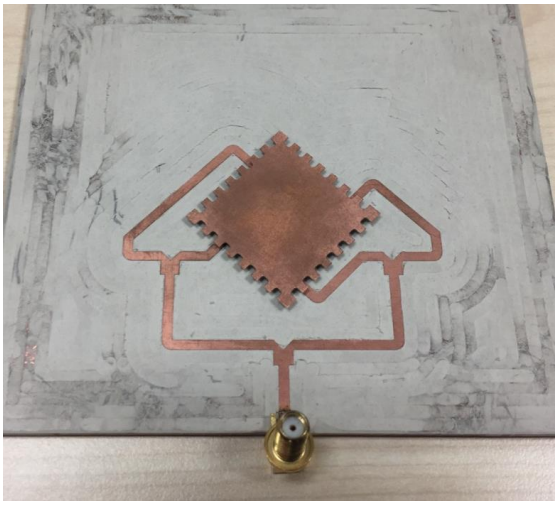

Figure 49. Realized structure for the 3rd mode excitation with T-junction

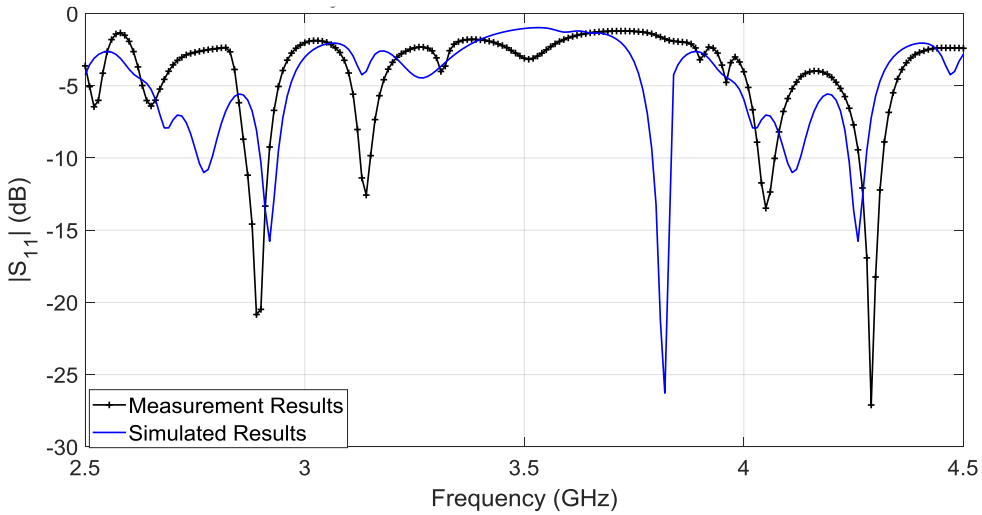

Figure 50. S_{11} vs. frequency of realized structure for the 3rd mode excitation

As it is seen in figure 50, the 3rd eigenmode resonance frequency does not match with the measurement results. It seems the excitation of this mode couldn't be achieved with such low resonance bandwidth values. 3% bandwidth seems too narrow for exciting the 3rd mode. Thus, the slots should have been smaller in number and they should have been more elliptical rather than having sharp corners as shown in Table 2. Still, a similar resonance to the 3rd mode at 4.2 GHz exists both in the simulations and the measurements. Note that, the 3rd mode patterns will be compared at 4.2 GHz in the next part.

3.2. Pattern Measurements

Figure 51 shows the relative positions of the antenna under test. All of the rotation direction and plane explanations given in the polar pattern drawings will be with respect to this reference coordinate system for the 1st mode. Also same reference coordinate system is shown in Figure 54 for the 3rd mode measurements.

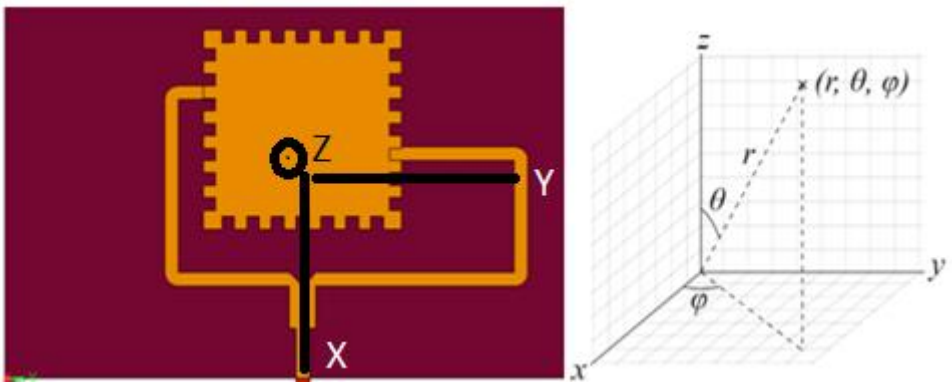

Figure 51. Coordinate system and reference planes for the 1st mode measurements

Figure 52 and Figure 53 compares the measured and simulated radiation patterns for E_θ and E_ϕ components, respectively. The main direction of radiation is at broadside with a 3-dB beamwidth about 60^0. Measurements are consistent with the simulations. Rather small discrepancies are considered to be due to similar non-ideal conditions such as ones in the fabrication stage and measurement environment.

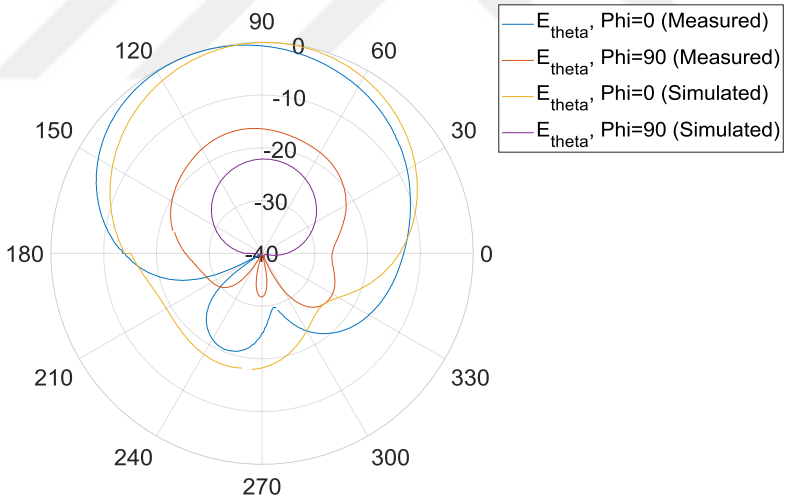

Figure 52. E_θ the 1st mode radiation pattern at 2.7 GHz

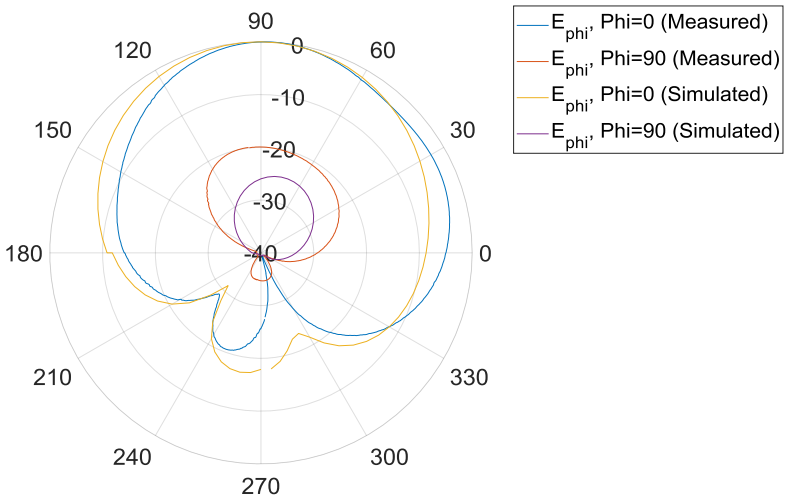

Figure 53. Eϕ the 1st mode radiation pattern at 2.7 GHz

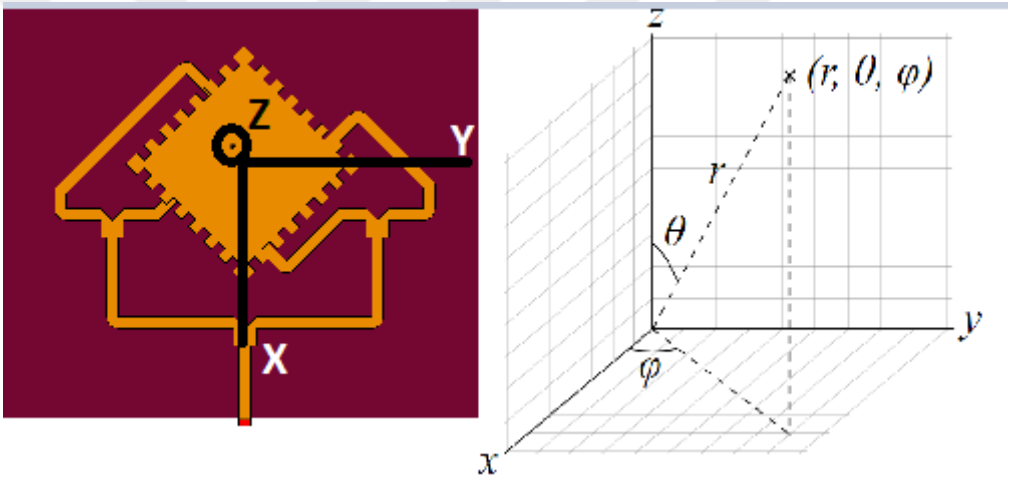

Figure 54: Coordinate system and reference planes for the 3rd mode measurements

The pattern measurements and simulation results for 3rd mode excitation are given in Figure 55 and Figure 56. Both of these measurements indicate a null at the broadside is obtained and main beams are tilted about 37^0 from broadside which was the main aim behind exciting this 3rd mode. Note that since both x-directed and y-directed currents are excited with equal amplitude in the 3rd mode, both E_θ and E_ϕ components are observed in two principle planes.

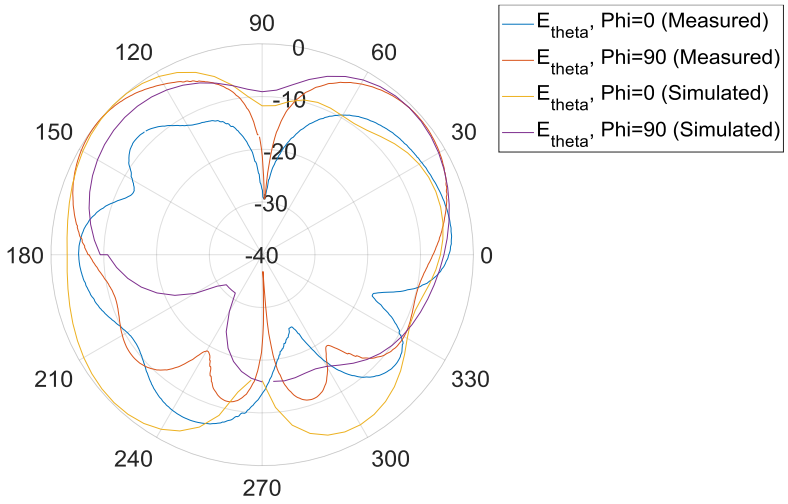

Figure 55. E_θ the 3rd mode's radiation pattern at 4.2 GHz

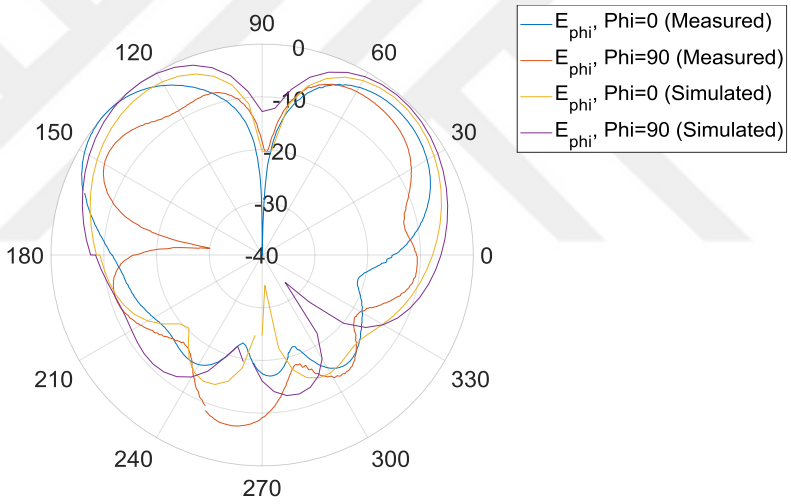

Figure 56. E_ϕ the 3rd mode radiation pattern at 4.2 GHz

CHAPTER 4

FUTURE WORKS AND CONCLUSIONS

4.1. Future Works

Instead of T-junctions, it is more convenient to use structures like ratrace couplers with PIN diode switches because of their phase shifting abilities. Not only that, but these couplers will also provide lower return loss and higher isolation between feeding branches. Sum and difference ports of these couplers naturally give out of phase outputs. So, there will be less need for line length adjustment for phase alignments.

Excitation of Different Eigenmodes Using Ratrace Couplers

The main reason using a ratrace coupler is its phase distribution between ports. One could divide the power equally by using different type of couplers as well such as branch line coupler. However, as it can be seen from its scattering matrix in Figure 57, the phase difference between its sum and difference ports are 180^0. And this is actually the phase difference required to excite different eigenmodes mentioned in previous sections.

The diagram of the ratrace coupler is shown in Figure 57.

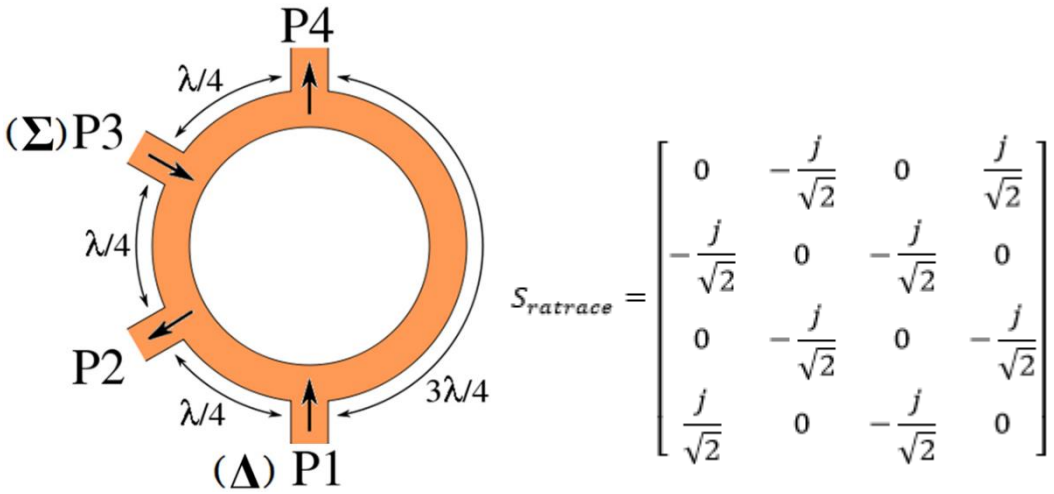

Figure 57. Sum and difference ports of ratrace coupler

Note that, when the 1st port is fed by a source the 2nd and the 4th ports will get equal power and phase difference of 180^0 if and only if the 3rd port is terminated with a matched load. Otherwise unwanted reflections will occur and this will disturb the matching. Figure 58 and Figure 59 show the simulated S parameters (both magnitude phase) of a ratrace coupler with a center frequency of 2.7 GHz. Recall that 2.7 GHz is the resonance frequency of the first two modes.

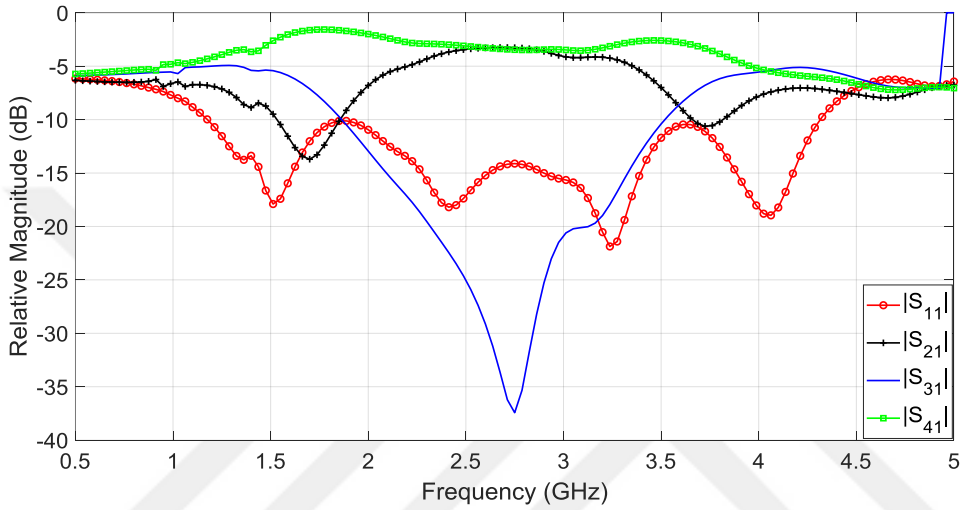

Figure 58. $|S_{n1}|$ vs. frequency of ratrace coupler designed for the 1st mode excitation

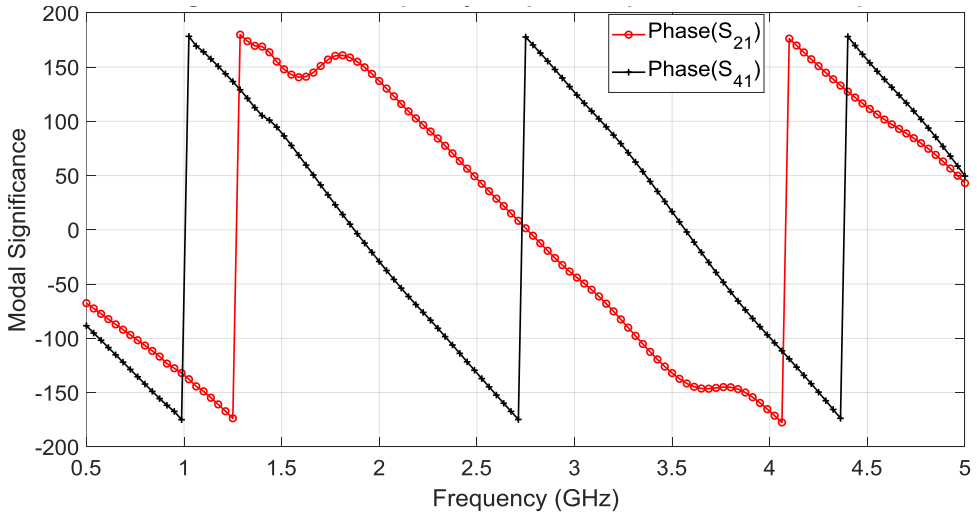

Figure 59. Phase of sum and difference ports vs. frequency

Excitation of the 1st mode using ratrace coupler feeding network

Having showed the S-parameters of the ratrace coupler, now it will be used in the feeding network for excitation of the 1st and the 2nd eigenmodes. Although the phase

difference at the output ports of the coupler is 180^0, the line lengths will slightly change it due to the feeding stub positions. So a length adjustment for phases on the feed lines just at the entrance of the patches is needed so that the 180^0 phase difference is maintained. But this will not be as drastic as in the case of T-junction divider. Figure 60 shows such a configuration for phase adjustments where difference port's vertical branch is kept shorter to compensate the phase shift. Also notice that, isolated port is terminated with a 50 Ω load to prevent unwanted reflections.

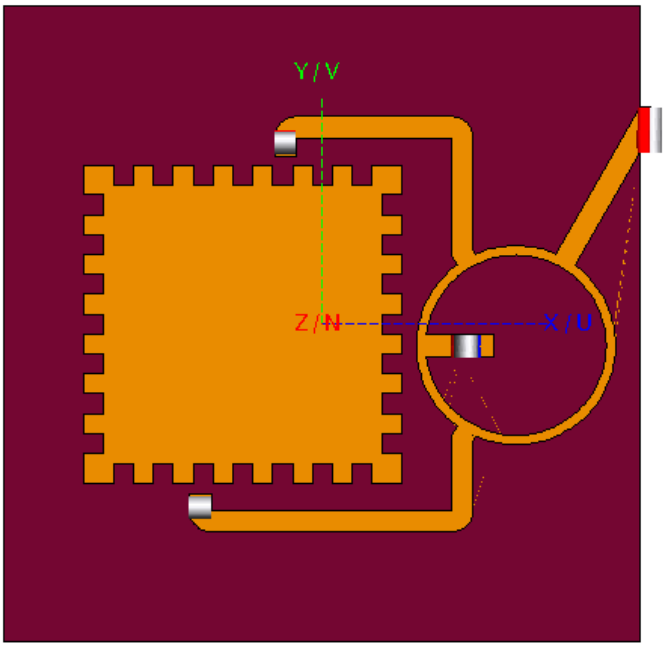

Figure 60. Ratrace coupler feeding scheme for the 1st mode

Figure 61 shows equal amplitude is maintained at the end of the feed points with a 3.8 dB loss and Figure 62 demonstrates the 180^0 phase shift between the ports is obtained.

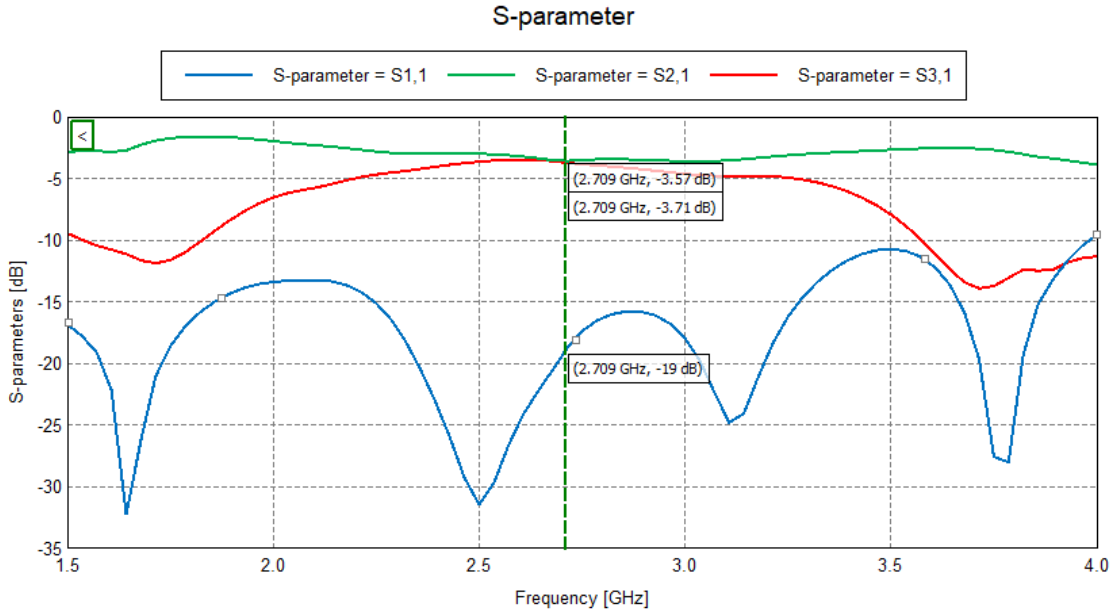

Figure 61. Magnitudes at the input ports for the 1st mode excitation scheme

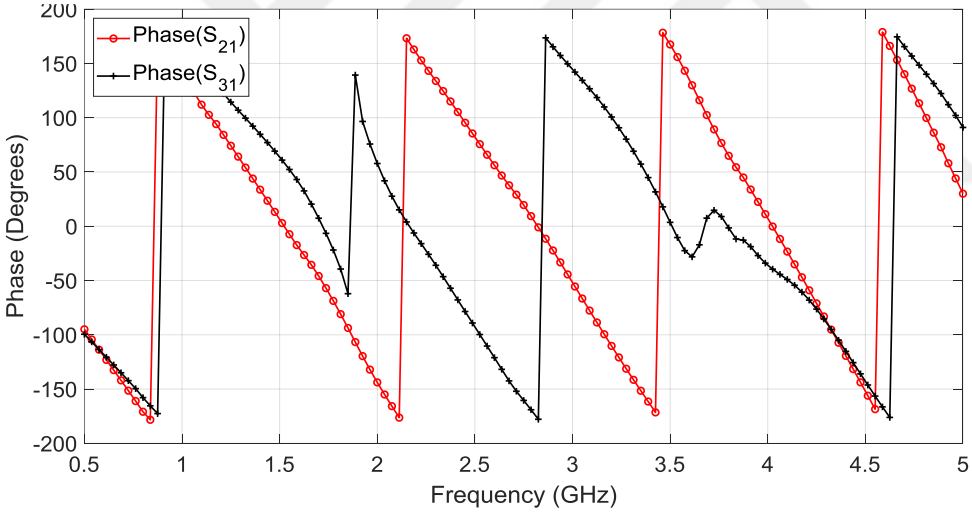

Figure 62. Phase distribution at the input ports for the 1st mode excitation scheme

Resulting current distribution and radiation patterns are given in Figure 63 and Figure 64 respectively and as it can be seen the radiation pattern matches with the 1st mode's pattern and exhibits a realized gain of 6 dBi at broadside.

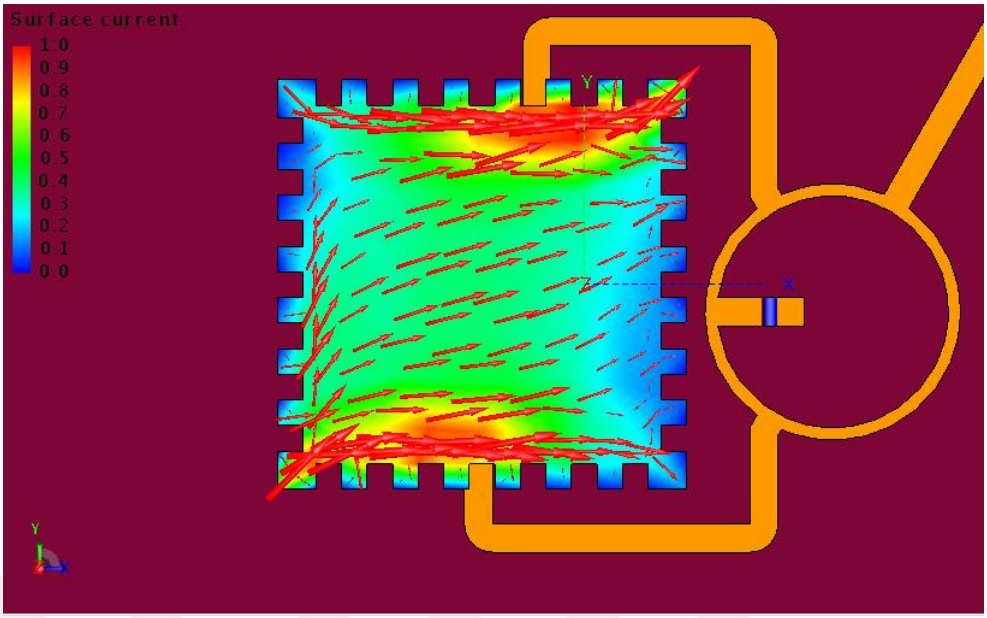

Figure 63. Current distribution for excitation of the 1st mode with ratrace coupler

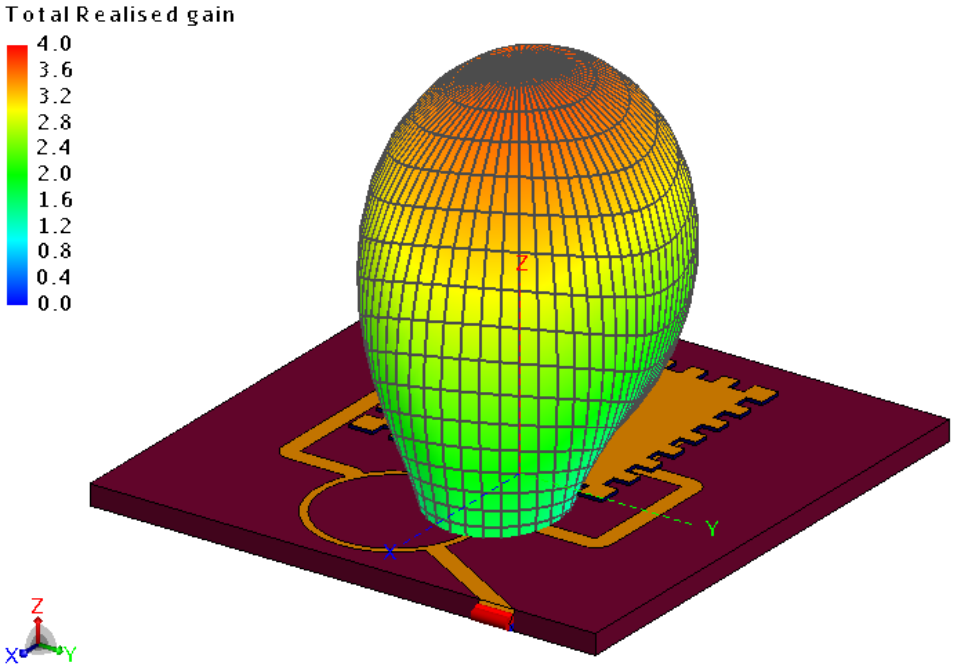

Figure 64. Radiation pattern for excitation of the 1st mode with ratrace coupler

Excitation of the 3rd eigenmode using ratrace coupler feeding network

To excite the 3rd eigenmode all four edges of the patch are fed as shown in Figure 65. As it is seen cascaded ratrace couplers are used to split the power.

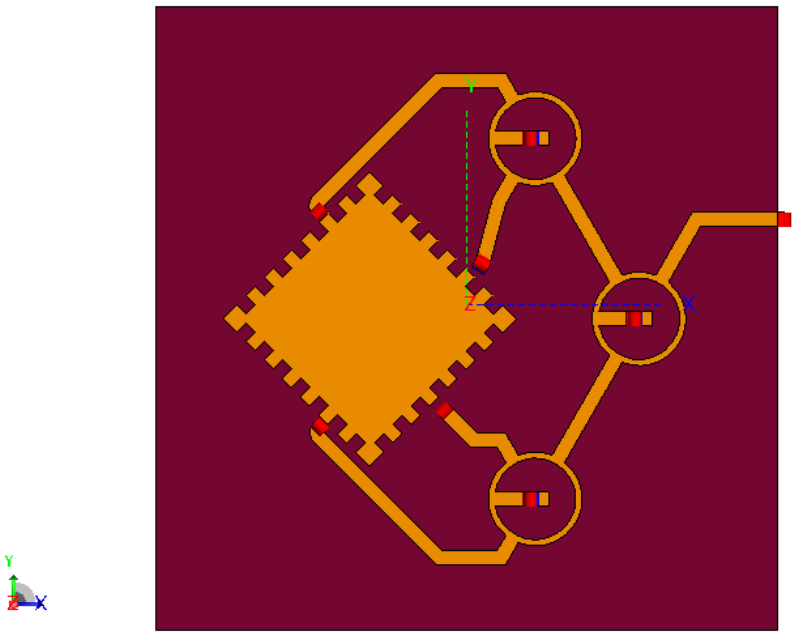

Figure 65. Cascaded ratrace couplers for the 3rd mode excitation

The same phase adjustment is implemented to decide feeding positions. The resulting magnitude and phase distributions are given in Figure 66 and Figure 67 respectively. Unfortunately, a magnitude imbalance occurs with this configuration as well. 0.75 dB fluctuation occurs with the opposing edges. And Figure 67 shows a 4^0 deviation from out of phase case. The effects of these imbalances will be observed in the radiation pattern again.

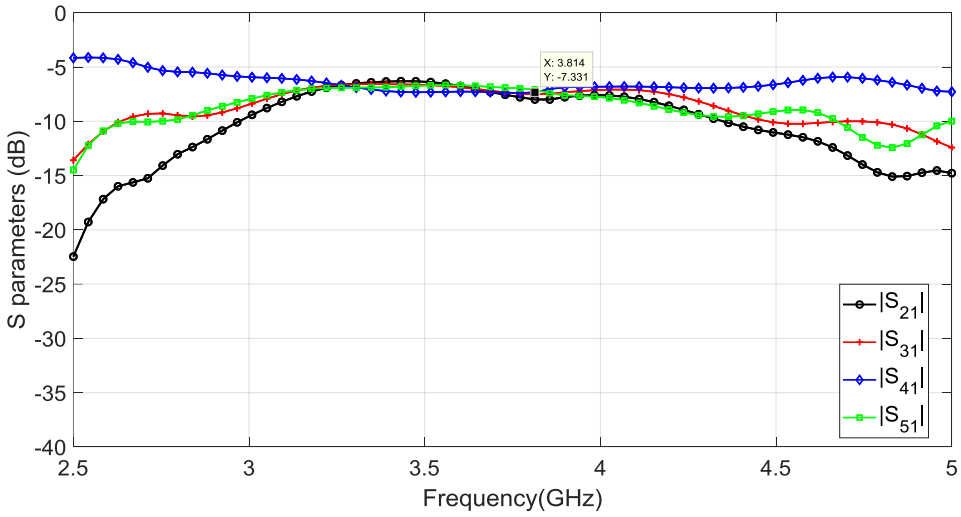

Figure 66. Magnitudes at the input ports for the 3rd mode excitation scheme

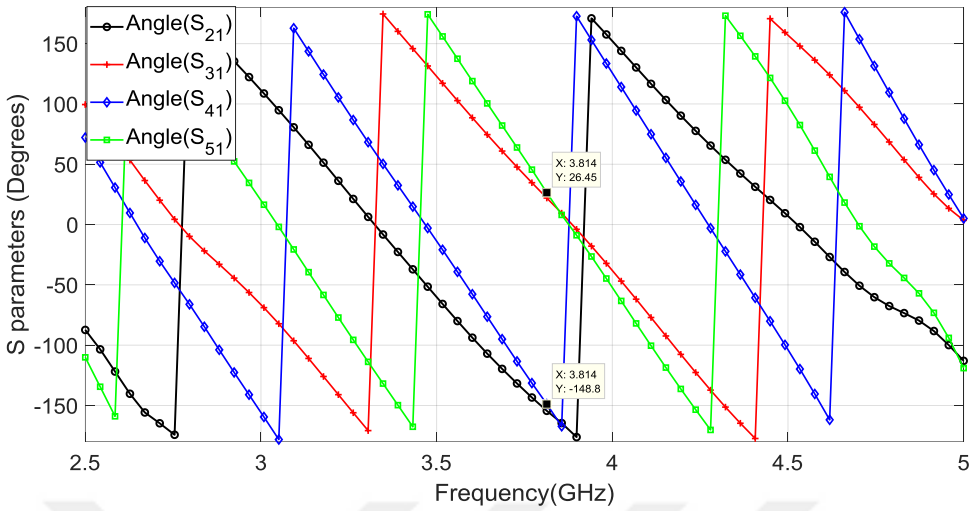

Figure 67. Cascaded ratrace couplers for the 3rd mode excitation

After the phase adjustments the resulting current distribution and radiation pattern is shown in Figure 68 and Figure 69, respectively. Although the current distribution is very similar to the 3rd mode, the slight difference in magnitudes and phases between the ports cause imbalance in the radiation pattern.

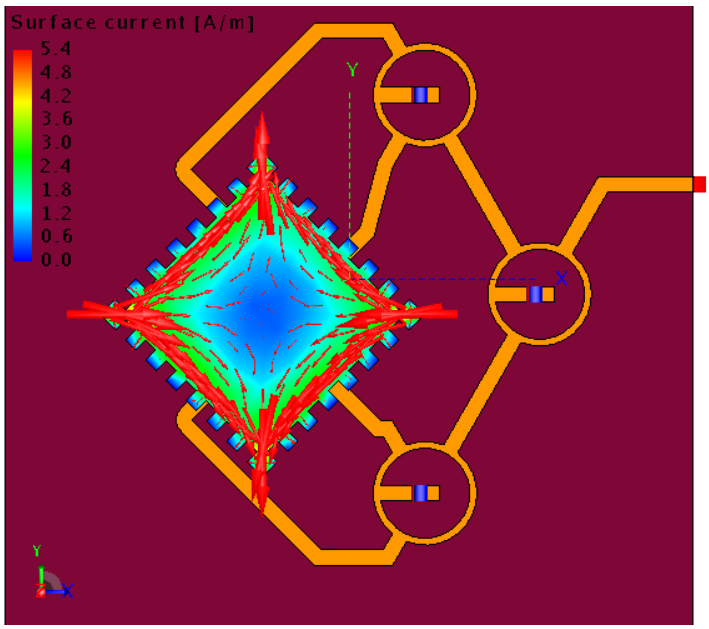

Figure 68. Current distribution for excitation of the 3rd mode with ratrace coupler

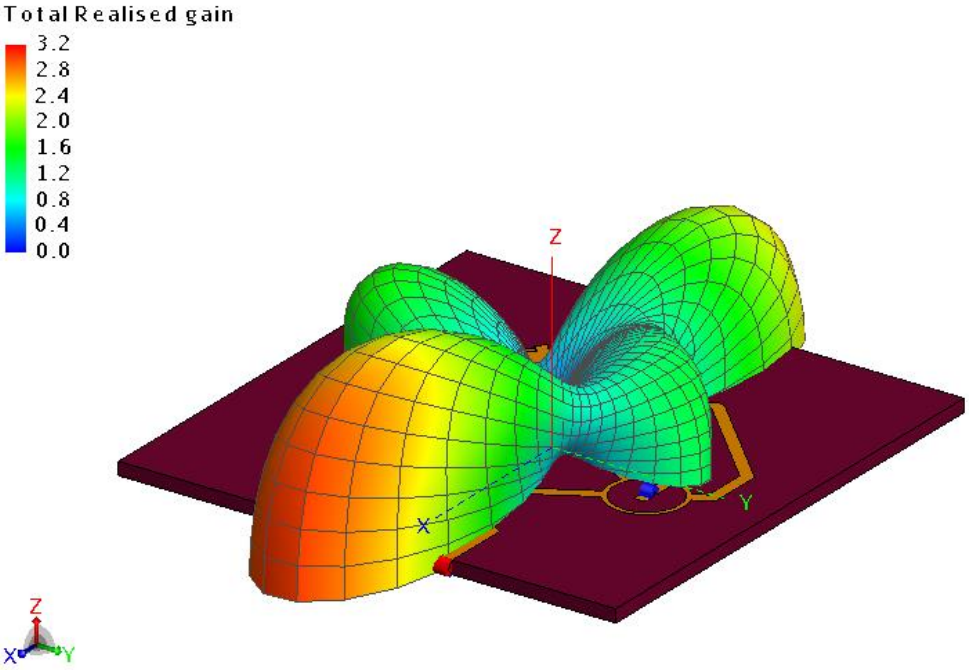

Figure 69. Radiation Pattern for excitation of the 3rd mode with ratrace coupler

4.2. Conclusions

In this thesis, application fields of pattern reconfigurable antennas have been studied. Different antenna synthesis techniques which make use of characteristic mode analysis have researched. Advantages and drawbacks of each method are discussed and it is shown that most works in the literature require additional conducting elements to reconfigure their patterns.

The main motivation and novelty of this work comes from aiming the excitation of multiple modes with a single element. The shape of a square patch is manipulated in order to have three orthogonal eigenmodes resonating at close at the same band of frequencies. Although it was shown that the resonant frequencies can be approached to each other, the trade-off between the bandwidth and frequency ratios prevents the three modes resonating at the same frequency. Instead each mode is excited at its own resonance.

Proximity coupled feed is used for ease of fabrication and miniaturization. Impedance matchings have been achieved by optimizing the stub lengths underneath the radiating patch. First, it was done using separate ports for the sake of simplicity in terms of phase adjustments. After deciding the stub lengths, the patch is fed from a single port for both mode excitation cases. T-junctions are used for dividing the power and phase adjustments at the end points of the feed are done by manipulating the line lengths. Low enough return loss and sufficient gains are obtained along with the desired pattern shapes on simulation. After fabrication, the measured return losses and patterns are compared with simulation results and expected results are obtained for the 1^{st} mode whereas some discrepancies observed for the 3^{rd} mode's excitation. The main resonance couldn't be excited at 3.8 GHz. 3% simulated bandwidth was a risk beforehand and unfortunately it turned out to be a non-resonant at expected frequency. Instead another common resonance at 4.2 GHz is compared in terms of radiation patterns. And they turned out to be consistent with 30^0 tilted beams.

Finally, another technique for feedings is proposed utilizing ratrace couplers. Desired matchings and radiation patterns obtained. The benefits and drawbacks of this method are discussed.

REFERENCES

[1] C. E. Shannon, "A symbolic analysis of relay and switching circuits," in *Transactions of the American Institute of Electrical Engineers*, vol. 57, no. 12, pp. 713-723, Dec. 1938, doi: 10.1109/T-AIEE.1938.5057767.

[2] Luther, J.J., Ebadi, S., ve Gong, X., "A Microstrip Patch Electronically Steerable Parasitic Array Radiator (ESPAR) Antenna with Reactance-Tuned Coupling and Maintained Resonance," *IEEE Transactions on Antennas and Propagation*, vol. 60, no. 4, pp. 1803–1813, 2012.

[3] X. Ding and B. Wang, "A Novel Wideband Antenna With Reconfigurable Broadside and Endfire Patterns," in *IEEE Antennas and Wireless Propagation Letters*, vol. 12, pp. 995-998, 2013, doi: 10.1109/LAWP.2013.2278139.

[4] S. Chen, P. Qin, W. Lin and Y. J. Guo, "Pattern-Reconfigurable Antenna With Five Switchable Beams in Elevation Plane," in *IEEE Antennas and Wireless Propagation Letters*, vol. 17, no. 3, pp. 454-457, March 2018, doi: 10.1109/LAWP.2018.2794990.

[5] Li, H., Lau, B.K., ve He, S., "Design of Closely Packed Pattern Reconfigurable Antenna Array for MIMO Terminals," IEEE Transactions on Antennas and Propagation, vol. 65, no. 9, pp. 4891–4896, 2017.

[6] T. Q. Tran and S. K. Sharma, "Radiation Characteristics of a Multimode Concentric Circular Microstrip Patch Antenna by Controlling Amplitude and Phase of Modes," in *IEEE Transactions on Antennas and Propagation*, vol. 60, no. 3, pp. 1601-1605, March 2012, doi: 10.1109/TAP.2011.2180305.

[7] W. Lin, H. Wong and R. W. Ziolkowski, "Wideband Pattern-Reconfigurable Antenna With Switchable Broadside and Conical Beams," in *IEEE Antennas and Wireless Propagation Letters*, vol. 16, pp. 2638-2641, 2017, doi: 10.1109/LAWP.2017.2738101.

[8] R. J. Garbacz, "A Generalized Expansion for Radiated and Scattered Fields," Ph.D. dissertation, Ohio State University, Columbus, 1968.

[9] R. F. Harrington and J. R. Mautz, "Theory of characteristic modes for conducting bodies," *IEEE Trans. Antennas Propag*., vol. AP-19, no. 5, pp. 622–628, Sep. 1971

[10] Cabedo Fabrés, M., "Systematic design of antennas using the theory of characteristic modes". *Ph.D. Dissertation*, Universitat Politècnica de València, 2007.

[11] D. Manteuffel and R. Martens, "Compact Multimode Multielement Antenna for Indoor UWB Massive MIMO," in *IEEE Transactions on Antennas and Propagation*, vol. 64, no. 7, pp. 2689-2697, July 2016, doi: 10.1109/TAP.2016.2537388..

[12] K. Li and Y. Shi, "A Pattern Reconfigurable MIMO Antenna Design Using Characteristic Modes," in *IEEE Access*, vol. 6, pp. 43526-43534, 2018, doi: 10.1109/ACCESS.2018.2863250.

[13] F. A. Dicandia, S. Genovesi and A. Monorchio, "Efficient Excitation of Characteristic Modes for Radiation Pattern Control by Using a Novel Balanced Inductive Coupling Element," in *IEEE Transactions on Antennas and Propagation*, vol. 66, no. 3, pp. 1102-1113, March 2018, doi: 10.1109/TAP.2018.2790046.

[14] R. Martens, E. Safin and D. Manteuffel, "Inductive and capacitive excitation of the characteristic modes of small terminals," *2011 Loughborough Antennas & Propagation Conference*, Loughborough, 2011, pp. 1-4, doi: 10.1109/LAPC.2011.6114141.

[15] K. Kumar Kishor and S. V. Hum, "A Pattern Reconfigurable Chassis-Mode MIMO Antenna," in *IEEE Transactions on Antennas and Propagation*, vol. 62, no. 6, pp. 3290-3298, June 2014, doi: 10.1109/TAP.2014.2313634.

[16] Z. Miers, H. Li and B. K. Lau, "Design of bezel antennas for multiband MIMO terminals using Characteristic Modes," *The 8th European Conference on Antennas and Propagation (EuCAP 2014)*, The Hague, 2014, pp. 2556-2560, doi: 10.1109/EuCAP.2014.6902342.

[17] Z. Mahlaoui, E. Antonino-Daviu, A. Latif and M. Ferrando-Bataller, "From the Characteristic Modes Analysis to the Design of a Radiation Pattern Reconfigurable Antenna," *2019 13th European Conference on Antennas and Propagation (EuCAP)*, Krakow, Poland, 2019, pp. 1-4.

[18] S. Dumanli, "On-body antenna with reconfigurable radiation pattern," *2014 IEEE MTT-S International Microwave Workshop Series on RF and Wireless Technologies for Biomedical and Healthcare Applications (IMWS-Bio2014)*, London, 2014, pp. 1-3, doi: 10.1109/IMWS-BIO.2014.7032385.

[19] Chaudhury, Shameem & Schroeder, Werner & Chaloupka, H.J.. (2007). MIMO antenna system based on orthogonality of the characteristic modes of a mobile device." 58 - 62. 10.1109/INICA.2007.4353932.

[20] FEKO User's Manual," Suite 2019, EM Software & Systems, South Africa, March 2019.

[21] RO4000 Series High Frequency Circuit Materials Data Sheet” ”, Rogers Corparation, Chandler, AZ, USA

[22] RT/duroid® 6010LM High Frequency Laminates Data Sheet”, Rogers Corparation, Chandler, AZ, USA

[23]Balanis, C., 2005. *Antenna Theory*. New York: Wiley-Interscience.

[24] V. Sharma, B. Sharma, V. K. Saxena, K. B. Sharma and D. Bhatnagar, "Modified rectangular patch antenna with air-gap for improved bandwidth," 2008 International Conference on Recent Advances in Microwave Theory and Applications, Jaipur, 2008, pp. 227-229, doi: 10.1109/AMTA.2008.4763098.

[25] LPKF ProtoMat S100 User Manual v. 2.0 2006”, Garbsen, Germany, LPKF Laser & Electronics AG

[26] Autodesk EAGLE User Manual v. 5.0 2010”, Florida, USA, Cadsoft Computer Inc.

[27] Keysight N2530A User Manual v. 1.0 2017”, LA, USA, Keysight Inc.

[28] Amphenol 132255-11 Edge Mount SMA Connector Datasheet